

An integrated mathematical model of the human cardiopulmonary system: model development

Antonio Albanese,¹ Limei Cheng,¹ Mauro Ursino,² and Nicolas W. Chbat^{1,3}

¹Philips Research North America, Briarcliff Manor, New York; ²Department of Electrical, Electronic, and Information Engineering, University of Bologna, Bologna, Italy; and ³Departments of Biomedical Engineering and Mechanical Engineering, Columbia University, New York, New York

Submitted 7 April 2014; accepted in final form 3 December 2015

Albanese A, Cheng L, Ursino M, Chbat NW. An integrated mathematical model of the human cardiopulmonary system: model development. *Am J Physiol Heart Circ Physiol* 310: H899–H921, 2016. First published December 18, 2015; doi:10.1152/ajpheart.00230.2014.—Several cardiovascular and pulmonary models have been proposed in the last few decades. However, very few have addressed the interactions between these two systems. Our group has developed an integrated cardiopulmonary model (CP Model) that mathematically describes the interactions between the cardiovascular and respiratory systems, along with their main short-term control mechanisms. The model has been compared with human and animal data taken from published literature. Due to the volume of the work, the paper is divided in two parts. The present paper is on model development and normophysiology, whereas the second is on the model's validation on hypoxic and hypercapnic conditions. The CP Model incorporates cardiovascular circulation, respiratory mechanics, tissue and alveolar gas exchange, as well as short-term neural control mechanisms acting on both the cardiovascular and the respiratory functions. The model is able to simulate physiological variables typically observed in adult humans under normal and pathological conditions and to explain the underlying mechanisms and dynamics.

cardiopulmonary model; cardiorespiratory interactions; respiratory control; cardiovascular control

NEW & NOTEWORTHY

This paper describes a novel integrated mathematical model of the cardiovascular and respiratory systems that includes the main cardiorespiratory interactions and short-term regulation mechanisms. Model results under normal resting conditions are similar to those observed in average populations.

LIFE DEPENDS ON THE INTERACTIONS between the cardiovascular and respiratory systems. The harmonious balance of such interactions maintains vital physiological variables, such as blood flow and blood oxygen (O_2) content, within specific ranges. The cardiovascular and respiratory systems in humans interact via several mechanisms, continuously, in a complex and nonlinear manner. O_2 and carbon dioxide (CO_2) are exchanged between pulmonary capillary blood and alveolar air, and the efficacy of such exchange depends on the success of their coupling. Furthermore, the amount of blood pumped by the heart and the degree of vessel vasoconstriction affect the blood gas transport delay, which is a key determinant of O_2 and CO_2 blood contents. These, in turn, modulate the depth and frequency of respiratory efforts via the action of specific receptors (chemoreceptors), which become active when O_2 and

CO_2 blood contents are out of their normal ranges. Mechanical interactions also exist, due to the fact that the chest contains the respiratory system and a significant portion of the cardiovascular system. These are particularly important during mechanical ventilation (MV), when elevated intrathoracic pressure could compromise ventricular filling and stroke volume, thus reducing arterial blood pressure (ABP). In turn, ABP modulates the activity of specific cardiovascular receptors (baroreceptors) that induce neural activity changes in both the sympathetic and parasympathetic branches of the autonomic nervous system (ANS), ultimately affecting heart rate (HR), cardiac contractility, and vasomotor tone. Mechanisms outside of the ANS control also exist. Local autoregulation and central nervous system (CNS) ischemic response are such examples. These become active in extreme conditions, such as severe hypoxia, to preserve perfusion and O_2 supply to vital organs (e.g., brain and coronary arteries).

Mathematical modeling and computer simulation can improve the understanding of such complex inter-relations and provide an efficient quantitative tool for the analysis and synthesis of cardiopulmonary dynamics. With the use of computer simulations, investigators can conduct virtual physiological experiments, test new hypotheses, and predict the effects of particular treatments or clinical maneuvers. Such simulations can be used in clinical decision making for diagnostic and therapeutic medicine.

Pioneering work in cardiorespiratory modeling was done by Grodins et al. (30, 31) in the 1950s and by Guyton and his coworkers (32) in the 1970s. However, due to the physiological knowledge and limited computational power of the time, the interactions between the cardiovascular and respiratory systems were not completely described. In the past few decades, thanks to the advancement in computational technology, scientific activity in this field has notably increased, and modeling complexity presented in the literature (9, 10, 13, 35–37, 41, 42, 44, 64, 67, 69) has grown to describe more accurately physiological mechanisms and their dynamics. However, the majority of these models is primarily either cardiovascular or pulmonary and thus does not permit a comprehensive exploration of a cardiopulmonary response to different acute conditions. Very few models have tried to address the strong dynamic interactions between the cardiovascular and respiratory systems, albeit with some limitations. For instance, the models by Magosso and Ursino (44) and Ursino and Magosso (69) [subsequently referred to as Ursino and Magosso (44, 69)] are, in our opinion, the most exhaustive in terms of the cardiovascular control mechanisms but lack respiratory and gas exchange components. The models by Cheng et al. (9, 10), which include Ursino and Magosso's (44, 69) cardiovascular system and

Address for reprint requests and other correspondence: N. W. Chbat, Philips Research North America, 345 Scarborough Rd., Briarcliff Manor, NY 10510 (e-mail: chbat@philips.com; chbat@columbia.edu).

control models, include a description of respiratory mechanics and gas exchange but are more focused on the interactions between sleep mechanisms and the ANS rather than on cardiorespiratory interactions. On the other hand, models by Lu et al. (41, 42) are detailed in their description of the mechanical interactions between the respiratory and cardiovascular systems and do include gas exchange but are less detailed in cardiovascular and respiratory neural control.

Our group has developed an integrated model to overcome some of the above limitations by including finer cardiorespiratory interactions and short-term control mechanisms. The model is the result of a multiyear effort, and only preliminary results have been presented in previous papers (2, 7, 27). The model is presented in two separate papers: Model development and Model validation under hypercapnia and hypoxia. The present (first) paper provides a rigorous description of the model, including results and comparison against human and animal data, in normal conditions, taken from literature. The companion (second) paper (8) includes validation against human data under hypercapnic and hypoxic conditions. The model incorporates essential features from existing models and represents a substantial extension of the models by Ursino and Magosso (44, 69). Their studies were mainly focused on analyzing the cardiovascular response to hypercapnic and hypoxic stimuli; the respiratory system was not explicitly considered. Arterial partial pressure of O₂ (PaO₂) and CO₂ (PaCO₂) was fed to the models as external inputs, and the gas exchange process was ignored completely. Here, separate submodels of respiratory mechanics, gas exchange in lungs and tissues, gas transport in blood, and respiratory control mechanisms have been added to attain an integrated cardiopulmonary model (CP Model) that is able to run in closed-loop mode, requiring inspiratory air gas content [fraction of inspired O₂ and CO₂ (FiO₂ and FICO₂, respectively)] and total blood volume as the only inputs. The model is able to generate physiological variable values typically observed in adult humans under normal, hypercapnic, and hypoxic conditions and explain the underlying mechanisms and dynamics. Furthermore, after further ad hoc validation, the model may be used to simulate different

disease conditions by appropriately varying parameter values before or during simulations, as well as therapeutic interventions.

METHODS

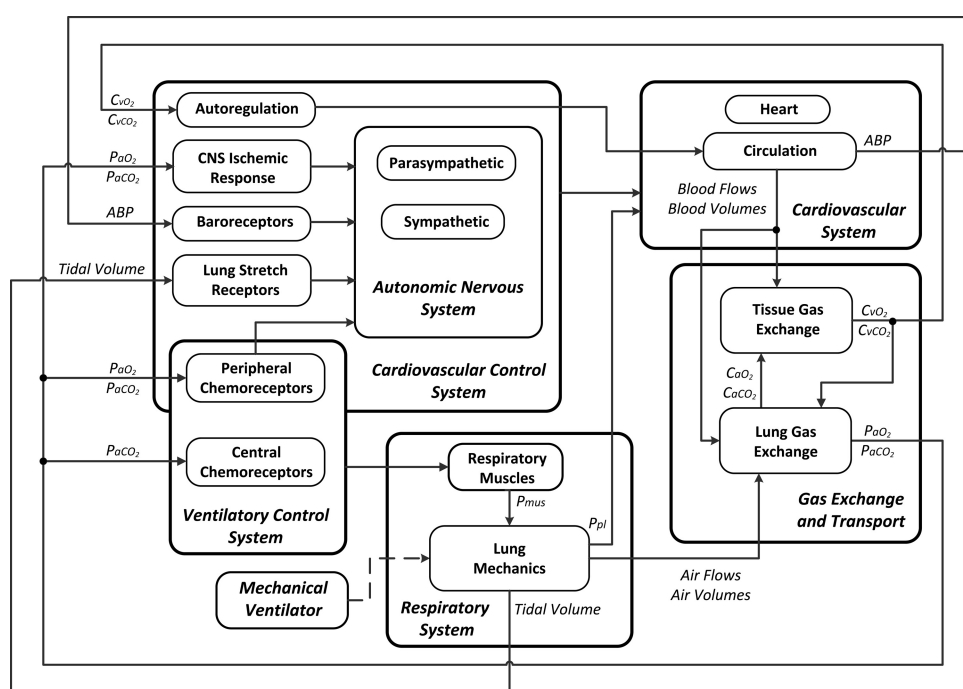
Model Development

The present CP Model incorporates cardiovascular circulation, respiratory mechanics, and gas exchange, along with their main short-term control mechanisms. A schematic block diagram of the model is shown in Fig. 1, where the interconnections among the different subsystems are highlighted. The cardiovascular system and the respiratory system interact via the gas exchange and transport module. This module describes the gas exchange processes in the lungs and the systemic tissues, along with the gas transport throughout the circulatory system. Both the cardiovascular and respiratory systems are subject to their own control mechanisms, identified in the block diagram as the Cardiovascular Control System and the Ventilatory Control System modules, respectively. Particularly, the cardiovascular function is regulated by the ANS that integrates the afferent information provided by the baroreceptor, peripheral chemoreceptor, and lung stretch receptor modules. Local autoregulation mechanisms are also included, along with a CNS-mediated response to acute ischemic conditions (CNS Ischemic Response). The respiratory function is assumed to be governed by the superposition of control mechanisms mediated by the peripheral chemoreceptors and the central chemoreceptors, which modulate the activity of the respiratory muscles acting on the lung mechanics module. This, in turn, can also be driven by the action of an external mechanical ventilator. In the following sections, a qualitative description of these different components is provided. Following a control-theory approach, the cardiovascular and respiratory systems are first described in the absence of regulatory actions (uncontrolled system). A description of their feedback control mechanisms is subsequently provided. A complete set of equations describing the model is presented in the APPENDIX.

The uncontrolled cardiovascular system model. The cardiovascular component of our CP Model is largely based on the work of Ursino and Magosso (44, 69). However, modifications were introduced, allowing more details of the heart-lung interactions and the integration of the cardiovascular module on one side and the lung mechanics



Fig. 1. Block diagram of the cardiopulmonary model (CP Model). CNS, central nervous system; CvO₂ and CvCO₂, oxygen (O₂) and carbon dioxide (CO₂) gas concentrations in the venous blood, respectively; PaO₂ and PaCO₂, O₂ and CO₂ arterial blood partial pressures, respectively; ABP, arterial blood pressure; P_{pl}, intrapleural pressure; P_{mus}, respiratory muscle pressure; CaO₂ and CaCO₂, O₂ and CO₂ gas concentrations in the arterial blood, respectively.



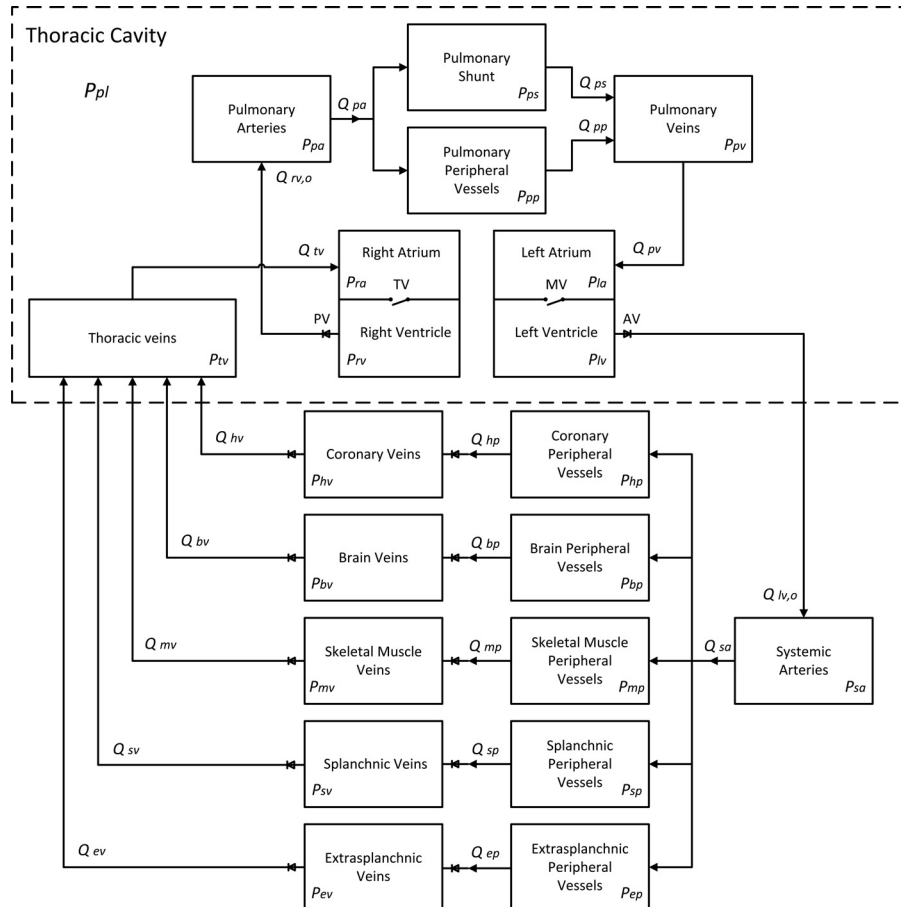


Fig. 2. Schematic diagram of the cardiovascular system model. P, pressure; Q, blood flow; MV, mitral valve; AV, aortic valve; TV, tricuspid valve; PV, pulmonary valve. Subscripts: la, left atrium; lv, left ventricle; lv, o, left-ventricle output; sa, systemic arteries; sp, splanchnic peripheral compartment; sv, splanchnic veins; ep, extrasplanchnic peripheral compartment; ev, extrasplanchnic veins; mp, skeletal muscle peripheral compartment; mv, skeletal muscle veins; bp, brain peripheral compartment; bv, brain veins; hp, coronary peripheral compartment; hv, coronary veins; tv, thoracic veins; ra, right atrium; rv, right ventricle; rv, o, right-ventricle output; pa, pulmonary artery; pp, pulmonary peripheral circulation; ps, pulmonary shunt; pv, pulmonary veins; pl, pleural space.

and gas exchange modules on the other. As shown in the schematic diagram in Fig. 2, the model includes a pulsatile heart, pulmonary circulation, and systemic circulation. The heart model includes both left and right hearts, along with their corresponding chambers (atria and ventricles) and valves (mitral, aortic, tricuspid, and pulmonary). The systemic circulation is subdivided into five districts, arranged in parallel, describing blood circulation into the coronary, brain, skeletal muscle, and splanchnic (comprising the liver, spleen, and gastrointestinal organs) and remaining extrasplanchnic (kidney, skin, bones, etc.) vascular beds. This distinction is necessary, since as will be described later, autonomic and local cardiovascular regulatory mechanisms exert different actions on each compartment. The hemodynamics in both systemic and pulmonary circulations distinguish among large arteries, peripheral vessels (combining arterioles and capillaries), and veins. The modifications, with respect to the original model formulation presented in Ursino and Magosso (44, 69), include the following additions. 1) A pulmonary shunt compartment has been added in parallel to the pulmonary peripheral circulation between the pulmonary artery and the pulmonary veins (anatomical shunting) to account for the amount of blood that does not pass through the pulmonary capillaries and hence, does not participate in gas exchange. 2) An additional compartment representing the thoracic veins, which return blood to the right atrium, has been included in the systemic circulation. 3) The effects of respiration on venous return (VR) and cardiac output (respiratory pump) have been modeled by considering intrapleural pressure (P_{pl}) as the reference extravascular pressure for those compartments that are located inside of the thoracic cavity (heart, lungs, and thoracic veins); all remaining compartments are assumed to be subject to extravascular atmospheric pressure (P_{atm}). 4) As a consequence of respiration, transmural pressure in the systemic veins can become negative at their point of entrance in the thoracic cavity; to account for this phenomenon, venous valves have been

included by inserting an ideal diode both upstream and downstream of each systemic venous compartment, thus preventing retrograde blood flow (45). With these modifications, the cardiovascular model includes a total of 20 compartments that are listed in Fig. 2.

The circulation model. Each vascular compartment shown in Fig. 2 is described through traditional windkessel models (67, 73), i.e., as the arrangement of a hydraulic resistance (R_j) that accounts for pressure energy losses and a hydraulic compliance (C_j) that determines the blood volume stored in each compartment at a given pressure. For those compartments where inertial forces in blood are relevant, i.e., the large pulmonary and systemic arteries, an inertance (L_j) is also included as a third parameter of the corresponding windkessel-type model. The general windkessel single-compartment model with L_j is illustrated in Fig. 3.

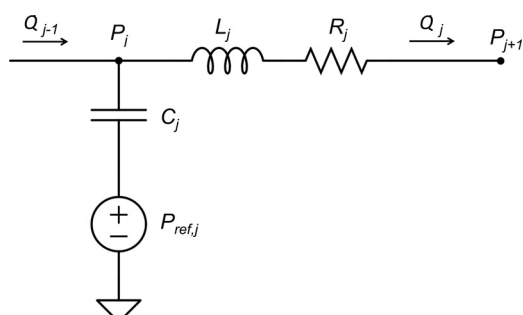


Fig. 3. Single-compartment, windkessel-type model. Q, outgoing blood flow rate; R, resistance; C, compliance; L, inertance; j, j + 1, j - 1, compartment index; P_{ref} , extravascular pressure reference (atmospheric pressure or P_{pl} , depending on the location of j).

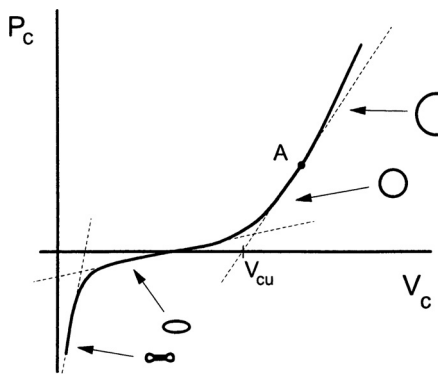


Fig. 4. Typical pressure–volume (PV) relationship of a blood vessel. P_c , transmural pressure; V_c , volume; V_{cu} , unstressed volume; A, normal operating point along the PV curve. Reproduced with permission from Timmons (65).

Equations relating pressures (P) and flows (Q) in the vascular system are obtained by enforcing conservation of mass principles for each vascular compartment of Fig. 2 (see APPENDIX). The pressure–volume (PV) relationship of each vascular compartment is assumed to be linear, except for the thoracic veins compartment. The assumption of a linear PV relationship allows constant and pressure-independent C_j . Hence, the volume of each of these compartments is computed as the sum of the unstressed component ($V_{u,j}$) and the excess volume component ($V_{e,j}$), which is associated with the increase in the transmural pressure

$$V_j = C_j \cdot P_{tm,j} + V_{u,j} \quad (1)$$

$\overbrace{\qquad\qquad\qquad}^{V_{e,j}}$

where $P_{tm,j}$ is the transmural pressure of the j th compartment. On the other hand, the thoracic veins compartment is modeled via a nonlinear, collapsible PV relationship. This choice can be justified by considering the typical PV relationship of a blood vessel shown in Fig. 4. It is quite linear near the unstressed volume (volume at 0 transmural pressure), concaves upward, gradually increases in slope at higher volumes, and concaves downward as the volume decreases and the vessel collapses (18). In arteries and capillaries, transmural pressure is typically high, and the operating point along the PV curve is such that a linear approximation is valid (17, 65). In contrast, in the venous circulation, the intravascular pressure is low; should any positive extravascular pressure exist, the vessel will collapse. This situation is most likely to occur in the thoracic veins, under the effects of a positive intrathoracic pressure (such as during MV). The nonlinear PV relationship of the thoracic veins compartment has been derived by combining features of slightly different PV curves proposed in the literature for the vena cava compartment (9, 49)

$$P_{tm,tv} = \begin{cases} D_1 + K_1 \cdot (V_{tv} - V_{u,tv}) - \psi & V_{tv} \geq V_{u,tv} \\ D_2 + K_2 \cdot e^{\frac{V_{tv}}{V_{tv,min}}} - \psi & V_{tv} < V_{u,tv} \end{cases} \quad (2)$$

with $\psi = K_{xp} / \left(e^{K_{xv}} - 1 \right)$

where $P_{tm,tv}$ and V_{tv} are the transmural pressure and volume of the thoracic veins compartment, respectively. The PV curve, corresponding to Eq. 2 (generated using the parameters seen in Table 2; and see Parameter Assignment), is shown in Fig. 5, from which the resemblance with the typical PV curve of Fig. 4 can be observed.

To account for the fact that when the vessel collapses, the blood flow toward that compartment is extremely reduced, the resistance of the thoracic veins compartment varies as a function of the volume, according to Lu et al. (41)

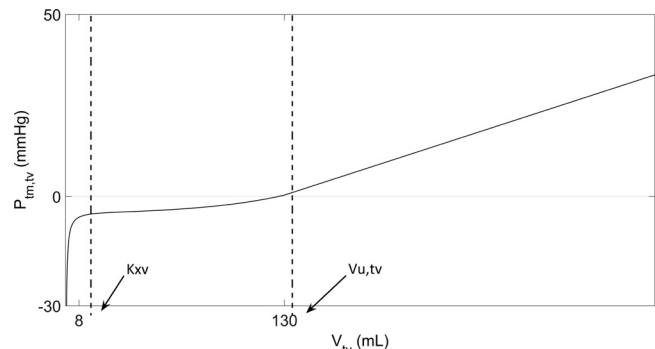


Fig. 5. PV relationship of the thoracic veins compartment according to Eq. 2. $P_{tm,tv}$, transmural pressure; V_{tv} , volume; $V_{u,tv}$, unstressed volume; K_{xv} , volume below which ψ becomes dominant.

$$R_{tv} = K_R \cdot \left(\frac{V_{tv,max}}{V_{tv}} \right)^2 + R_{tv,0} \quad (3)$$

where K_R is a scaling factor, $V_{tv,max}$ is the maximum volume, and $R_{tv,0}$ is an offset parameter. All of the remaining resistances of the vascular system have been assumed constant, with the exception of those of the systemic peripheral compartments that are assumed to vary under the action of feedback regulatory mechanisms (see The cardiovascular control model).

The effects of gravity on the cardiovascular system have been neglected. Hence, the model is suitable for simulating subjects in the supine position only, when the gravitational effects on the hydrostatic pressure gradient across the transverse axis of the body are negligible compared with the vertical axis gradient present in the upright position. Finally, note that in solving the model equations for the pressure variables, P_{atm} has been assumed to be zero, and hence, the resulting values of intravascular pressure in the j th compartment (P_j) in Fig. 3 represent above-atmospheric values.

The heart model The model of the pulsatile heart remains unchanged compared with that one used in Ursino and Magosso (44, 69), where an accurate description can be found. The only modification introduced is the inclusion of the P_{pl} as the external reference pressure acting outside of the heart chambers.

The respiratory system model As shown in Fig. 1, the model of the respiratory system includes the descriptions of the lung mechanics and the respiratory muscles. The tidal-breathing lung mechanics model is based on previous work by Rideout (55) and Fukui (26) and has been modified to include chest-wall and P_{pl} dynamics. Figure 6 shows the equivalent pneumatic circuit representing the lung mechanics model. It consists of the series arrangements of four segments, namely the larynx, trachea, bronchea, and alveoli. Each segment has been represented by a linear resistance and a linear compliance, which describe the dissipative and elastic forces that act on the respiratory system during normal breathing. Inertial forces have not been considered because they have negligible effects within the physiological breathing frequencies (50). The model can be driven by either an external pressure P_{vent} , representing the pressure provided by the ventilator, as in the case of mechanically ventilated patients, or by an internal generator P_{mus} , representing the pressure generated by the respiratory muscles, as in the case of spontaneously breathing patients. The chest wall has been modeled as a passive compliant element whose PV characteristic has been assumed linear and hence, described by a constant compliance term, chest-wall compliance (C_{cw}). This is a good approximation in the volume range of quiet breathing (2.5–3 liters), according to the typical assumption of a sigmoidal PV relationship (6). The chest-wall viscous resistance to flow has been neglected, as this typically has a small contribution to the overall respiratory system resistance in both healthy and diseased states (23, 29). The respiratory muscle generator is connected to the C_{cw} , which

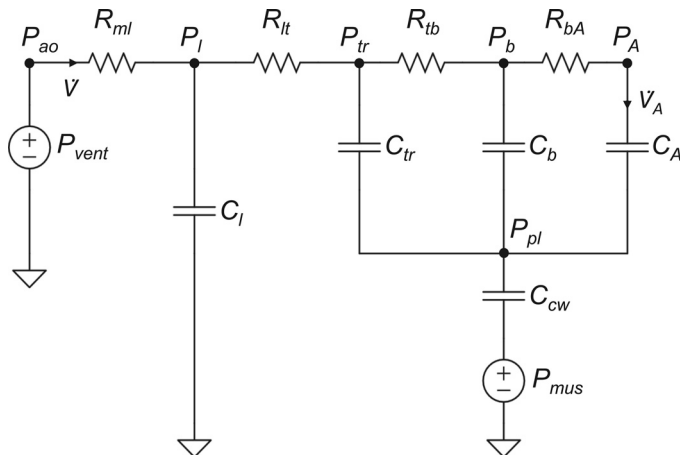


Fig. 6. Lung mechanics model. \dot{V} , total airflow; \dot{V}_A , alveolar airflow; P_{vent} , pressure provided by the ventilator. Subscripts: ao, airway opening; ml, mouth to larynx; l, larynx; lt, larynx to trachea; tr, trachea; tb, trachea to bronchea; b, bronchea; bA, bronchea to alveoli; A, alveoli; cw, chest wall.

acts on the pleural space, whose internal P_{pl} is transferred to those segments lying within the chest cavity, i.e., trachea, bronchea, and alveoli.

In the present study, since the model was used to simulate spontaneous breathing conditions, the action of the P_{vent} is nullified, and the airway opening pressure (P_{ao}) is always assumed to be equal to P_{atm} . However, the P_{vent} could be applied to simulate artificial ventilation conditions or even superimposed to the action of the P_{mus} to account for simultaneously natural and artificial breathing.

The P_{mus} has been modeled based on the average profile proposed by Mecklenburgh and Mapleson (46). This has been reproduced as a piece-wise, continuous function, consisting of an inspiratory parabolic profile and an exponential expiratory profile. Particularly, under the assumption of complete passive exhalation with no recruitment of the expiratory muscles [reasonable for minute ventilation (V_e) values up to 40 l/min (15)], P_{mus} is assumed to decrease from zero to its minimum end-inspiratory value during the inhalation phase and to return gradually to zero during exhalation, according to

$$P_{mus}(t) = \begin{cases} \frac{-P_{mus,min}}{T_I \cdot T_E} \cdot t^2 + \frac{P_{mus,min} \cdot T}{T_I \cdot T_E} \cdot t & t \in [0, T_I] \\ \frac{P_{mus,min}}{1 - e^{-\frac{T_E}{\tau}}} \cdot \left(e^{-\frac{(t-T_I)}{\tau}} - e^{-\frac{T_E}{\tau}} \right) & t \in [T_I, T] \end{cases} \quad (4)$$

where T_I and T_E represent the duration of the inspiratory and expiratory phases, respectively, T is the respiratory period, $P_{mus,min}$ is the minimum end-inspiratory pressure value representing the amplitude of the inspiratory efforts, and τ is the time constant of the exponential expiratory profile. The inspiratory and expiratory times are considered fixed fractions of T

$$\begin{aligned} T_I + T_E &= T = 60/RR \\ T_I &= T_E \cdot IE_{ratio} \end{aligned} \quad (5)$$

where RR is the respiratory rate (expressed in breaths/min) and IE_{ratio} is the inspiratory-expiratory time ratio. The muscle pressure waveform is repeated with the respiratory period. The expiratory P_{mus} is assumed to be directly proportional to the T_E , and IE_{ratio} is assumed to be fixed during a simulation. Hence, the P_{mus} profile is fully parameterized via the two quantities RR and $P_{mus,min}$, whose values are assumed to vary from breath to breath and are computed at the beginning of each respiratory cycle as output of the chemoreceptors module (see The respiratory control model).

Outputs of the lung mechanics model are the instantaneous pressures and volumes of each compartment, along with the instantaneous airflow into and out of them. The equations for pressures and flows are obtained by solving the electrical circuit shown in Fig. 6, based on conservation of mass principles. Volumes are then computed, taking into account the unstressed components (see Eq. 1). To allow interaction between the lung mechanics and the gas exchange model (see Fig. 1), the dead space is also considered, and its instantaneous volume is computed as the sum of the volumes of the three compartments that do not participate in gas exchange, i.e., larynx, trachea, and bronchea. Hence, differently from the majority of the models available in literature (9, 71), dead space is not assumed to be rigid, but its volume is constantly changing throughout a respiratory cycle. As a consequence of the elastic dead-space assumption, part of the total airflow entering the lung, denoted as \dot{V} , is spent to inflate the dead space and does not contribute to the effective flow that reaches the alveoli, denoted as \dot{V}_A . Furthermore, since the difference between the volumes of O_2 and CO_2 that are exchanged between alveoli and pulmonary capillary over a respiratory cycle is typically very small, the net airflow that is transferred from the alveoli to the pulmonary blood is neglected, and the inhaled tidal volume (V_T) over a respiratory cycle is assumed exactly equal to the corresponding exhaled V_T .

The gas exchange and transport model. The model of gas exchange and transport describes the O_2 and CO_2 exchange between pulmonary capillaries and lungs and between systemic capillaries and tissues, along with O_2 and CO_2 transport by blood throughout the circulatory system. As shown in the block diagram of Fig. 7, the model is made of three components, namely the Lung Gas Exchange, the Tissue Gas Exchange, and the Venous Pool Gas Transport. Circulatory transport delays are included in the model to account for the time that it takes for blood to transport gases from the lungs to the systemic tissues and from the thoracic veins back to the pulmonary capillaries (τ_{LT} and τ_{VL} , respectively). Gas transport throughout the venous pool is instead explicitly modeled, since blood flow in the venous section is typically slow, and hence, this section accounts for most of the circulatory blood transport delay. Only O_2 and CO_2 gas species are considered in the model, with nitrogen and other air gas components neglected. In the following, a detailed description of the three submodels is provided.

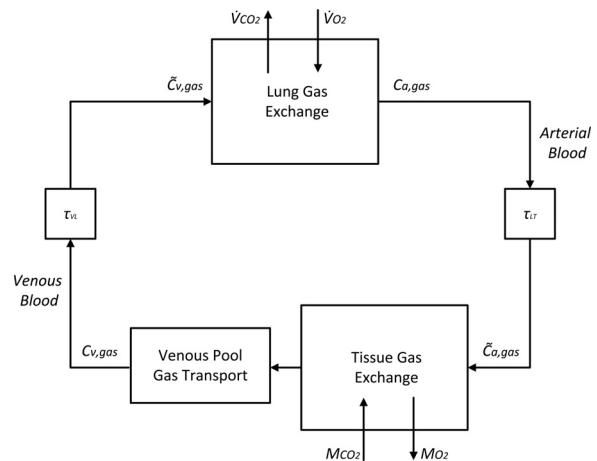


Fig. 7. Schematic diagram of the gas exchange and transport model highlighting the alveolar and tissue components, the venous pool gas transport block, and the blood transport delays. $C_{a,gas}$, arterial blood gas concentrations; $C_{v,gas}$, mixed venous blood gas concentrations; τ_{LT} , transport delay from lungs to systemic tissues; τ_{VL} , transport delay from thoracic veins to lungs; $\bar{C}_{v,gas}$, gas concentrations in the blood that enters the lung gas exchanger; $\dot{V}O_2$ and $\dot{V}CO_2$, O_2 and CO_2 gas flow between alveoli and pulmonary capillaries, respectively; M_{O_2} and M_{CO_2} , metabolic O_2 consumption and CO_2 production rates in the systemic tissues, respectively. The subscript gas indicates either O_2 or CO_2 .

The lung gas exchange. The lung gas exchange model includes anatomical dead space, alveoli, pulmonary capillaries (also belonging to the pulmonary peripheral compartment of the cardiovascular system), and right to left pulmonary shunts. A schematic block diagram is shown in Fig. 8. It receives V_D , V_A , and dead-space and alveolar volume (V_D and V_A , respectively) as inputs from the lung mechanics model, and pulmonary peripheral volume (V_{pp}) and blood flow through the pulmonary beds [pulmonary artery, peripheral circulation, and shunt (Q_{pa} , Q_{pp} , and Q_{ps})] as inputs from the cardiovascular model. Furthermore, the lung gas exchange model is obviously interconnected to the tissue gas exchange model, as shown in Fig. 7, as it requires as inputs the delayed venous gas concentrations in the blood that enter the lung gas exchanger ($\bar{C}_{v,gas}$) as well (where gas indicates either O_2 and CO_2). External inputs to the lung gas exchange model are the gas fractions in the inspired air ($F_{i,gas}$). Outputs of the model are the concentrations of gas in the pulmonary capillaries ($C_{pp,gas}$), which are then converted into arterial blood gas concentrations ($C_{a,gas}$). These are computed by applying conservation of mass to each of the three compartments in Fig. 8 for each gas species and assuming that every compartment is homogenous and perfectly mixed. Gases are assumed to be ideal, and gas fractions in the lungs are related to their corresponding partial pressures via the ideal gas law. Blood gas concentrations are related to their corresponding partial pressures via empirical dissociation curves (60) that are easily invertible and have been validated and used in previous cardiopulmonary models. These dissociation functions take into account both the Haldane and the Bohr effects. Finally, equilibrium between pulmonary capillaries and alveoli in terms of gas partial pressures is assumed to happen instantaneously. The complete set of equations governing the lung gas exchange model is reported in the APPENDIX.

The tissue gas exchange and venous pool gas transport. The tissue gas exchange model accounts for the O_2 consumption and CO_2 production of tissues and organs at the level of the systemic capillaries, whereas the venous pool gas transport model describes O_2 and CO_2 transport through the systemic and thoracic veins. A schematic diagram of the combined model is shown in Fig. 9. The model receives as input the delayed arterial gas concentrations from the lung gas exchange model ($\bar{C}_{a,gas}$) and provides as output the gas concentrations in the mixed venous blood ($C_{v,gas}$), computed at the exit of the thoracic veins compartment. Furthermore, the tissue gas exchange model is connected with the cardiovascular model, since it requires blood flows and volumes in the different systemic vascular beds as input as well. As shown in Fig. 9, tissue gas exchange is assumed to happen at the level of the five systemic peripheral compartments (coronary, brain, skeletal muscle, splanchnic, and extrasplanchnic).

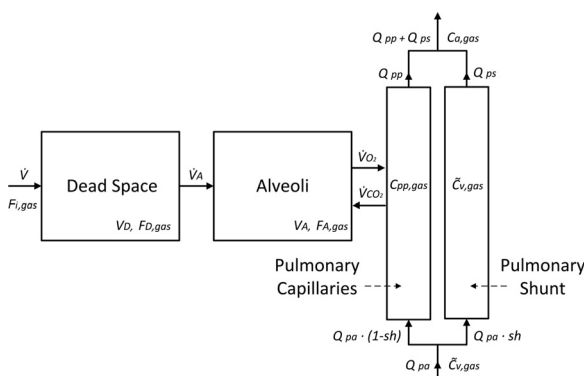


Fig. 8. Schematic diagram of the lung gas exchange model. V_D , dead-space volume; V_A , alveolar volume; $F_{i,gas}$, gas fractions in the inspired air; $F_{D,gas}$, gas fractions in the dead space; $F_{A,gas}$, gas fractions in the alveoli; $C_{pp,gas}$, gas concentrations in the pulmonary capillaries; Q_{pa} , blood flow from the pulmonary arteries; sh, shunt percentage; Q_{pp} , blood flow at the exit of the pulmonary capillaries; Q_{ps} , blood flow at the exit of the pulmonary shunt compartment.

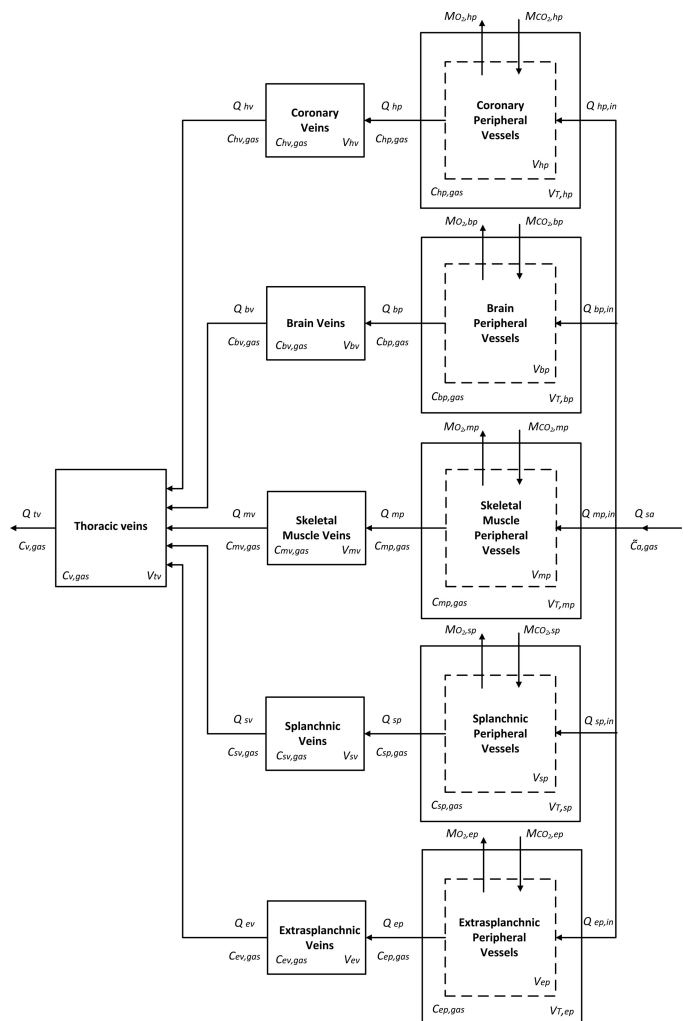


Fig. 9. Schematic diagram of the tissue gas exchange and venous pool gas transport model. $C_{jp,gas}$, gas concentration in the j th combined blood-tissue compartment; $C_{jv,gas}$, gas concentrations in the j th systemic venous compartment; Q_{sa} , blood flow at the exit of the systemic arteries; $Q_{jp,in}$, blood flow at the entrance of the j th systemic peripheral compartment; Q_{jp} , blood flow at the exit of the j th systemic peripheral compartment; Q_{jv} , blood flow at the exit of the j th systemic venous compartment; Q_{tv} , blood flow at the exit of the thoracic veins; V_{jp} , blood volume contained in the j th systemic peripheral compartment; $V_{T,jp}$, blood volume contained in the j th tissue compartment; V_{jv} , blood volume contained in the j th systemic venous compartment; V_{tv} , blood volume contained in the thoracic veins; $MO_{2;jp}$ and $MCO_{2;jp}$, O_2 consumption and CO_2 production rates in the j th blood-tissue compartment, respectively.

Each compartment supplies blood to an organ/tissue (or group of organs/tissues) that is modeled as a simple container, characterized by a constant tissue volume ($V_{T,jp}$), where the subscript jp indicates the j th systemic peripheral compartment. Blood and tissues are assumed to form a combined homogenous blood-tissue compartment that is characterized by gas concentrations $C_{jp,gas}$ and total volume given by the sum of the $V_{T,jp}$ and the blood volume V_{jp} of the corresponding systemic peripheral compartment by which it is supplied. Metabolic O_2 consumption and CO_2 production are assumed to happen within these combined blood-tissue compartments at constant rates in the systemic tissues of the j th systemic peripheral compartment ($MO_{2;jp}$ and $MCO_{2;jp}$), respectively. $C_{v,gas}$ is computed by applying conservation of mass principles to each compartment shown in Fig. 9 under perfectly mixed phase assumption and considering that $MO_{2;jp}$ and $MCO_{2;jp}$ are set. The complete set of equations governing the model is reported in the APPENDIX.

The cardiovascular control model. The cardiovascular control model includes the main short-term regulation mechanisms (time duration <1–2 min) that act on the cardiovascular function in response to acute hemodynamic and blood gas composition perturbations. The model is based on the previous work of Ursino and Magosso (44, 69), and a high-level schematic block diagram highlighting its input-output interconnections is shown in Fig. 10. Briefly, the model includes the action of carotid sinus baroreceptors, peripheral chemoreceptors, lung stretch receptors, autoregulation mechanisms, and a CNS directly mediated ischemic response. The afferent information coming from baroreceptors, chemoreceptors, and lung stretch receptors is first processed at the level of the ANS, which in turn, modulates sympathetic and parasympathetic activities in the neural efferent pathways. Sympathetic and parasympathetic neural fibers then control the cardiovascular system via modifications of heart period (HP), maximum ventricular contractilities ($E_{max,lv}$ and $E_{max,rv}$), resistances of the systemic peripheral beds (R_{hp}), and systemic venous unstressed volumes ($V_{u,jp}$). The HP is assumed to depend on a balance between sympathetic and parasympathetic activities, whereas all other effectors are assumed under the control of sympathetic fibers only. Circulation in the most vital vascular beds, i.e., the coronary and brain compartments, is assumed to be independent of the ANS modulation, only affected by local autoregulation mechanisms. Finally, the effect of a CNS ischemic response is modeled by assuming that PaO_2 and $PaCO_2$ can alter the sensitivity of the efferent sympathetic fibers to the stimuli coming from the afferent receptors (baroreceptors, chemoreceptors, and lung stretch receptors).

The mathematical equations governing the model have been taken from Ursino and Magosso (44, 69), where a detailed explanation can be found. However, the equations pertaining to the afferent peripheral chemoreceptors pathway (see Fig. 10) have been replaced with a more detailed model proposed in Ursino and Magosso (68). Motivations for this choice have been reported in a previous paper (2), and more details are included in the next section, since this model is also used in the respiratory control module.

The respiratory control model. The respiratory control model includes both the peripheral and central chemoreceptors. Reflexes arising from mechanoreceptors, such as the Hering-Breuer reflexes, are not taken into account, as these are believed to play a major role

only at high V_T . A schematic block diagram of the model is shown in Fig. 11. The central chemoreceptors are assumed to be sensitive to $PaCO_2$, whereas the peripheral chemoreceptors are assumed to be sensitive to both PaO_2 and $PaCO_2$. The central and peripheral chemoreceptors directly affect the RR and the amplitude of the respiratory muscle pressure generator, $P_{mus,min}$ (see The respiratory system model). This inclusion is an essential feature that differentiates our integrated CP Model from other large-scale models presented in literature. The majority of these models, in fact, assumes that chemoreceptors act on the respiratory system by directly changing V_e (9, 11, 44, 70) or by modifying V_T and RR (19, 20), hence ultimately affecting V_e . In these models, a set of static or dynamic equations coupling PaO_2 and $PaCO_2$ (or some surrogates of these variables) to V_e (or V_T and RR) is used to describe the entire respiratory control system, bypassing the physiological link between chemoreceptors and respiratory muscles. Very few models account for the relationship between blood gas contents and respiratory efforts (26, 42, 43), expressed in terms of P_{pl} or P_{mus} , and even fewer make a distinction between mechanisms affecting respiratory effort amplitude and mechanisms affecting respiratory rate (42, 43).

As supported by experimental studies performed on humans (61), there is no active interaction included in the model between the two distinct central and peripheral chemoreceptor mechanisms. Hence, the central and the peripheral contributions to the ventilation response, in terms of variations in RR and $P_{mus,min}$, are assumed to be additive. Contributions from the chemoreceptors are then added to the basal values of RR and $P_{mus,min}$ (RR_0 and $P_{mus,min0}$), generated by the intrinsic respiratory rhythm generator that produces a wakefulness drive when chemoreceptors are not stimulated.

A detailed description of the input-output relationships of the central and peripheral chemoreflex has been provided in a previous paper (2), and complete equations are reported in the APPENDIX. Briefly, the central chemoreceptor mechanism is described as a first-order dynamic system with a pure delay, having as input the variation of partial pressure of CO_2 (PCO_2) in the arterial blood with respect to a set-point value $PaCO_{2,n}$. The peripheral chemoreflex, on the other hand, is described as a two-stage transduction mechanism, where PaO_2 and $PaCO_2$ are first transduced into electrical activity of the peripheral chemoreceptor fibers, f_{apc} , which is then converted into

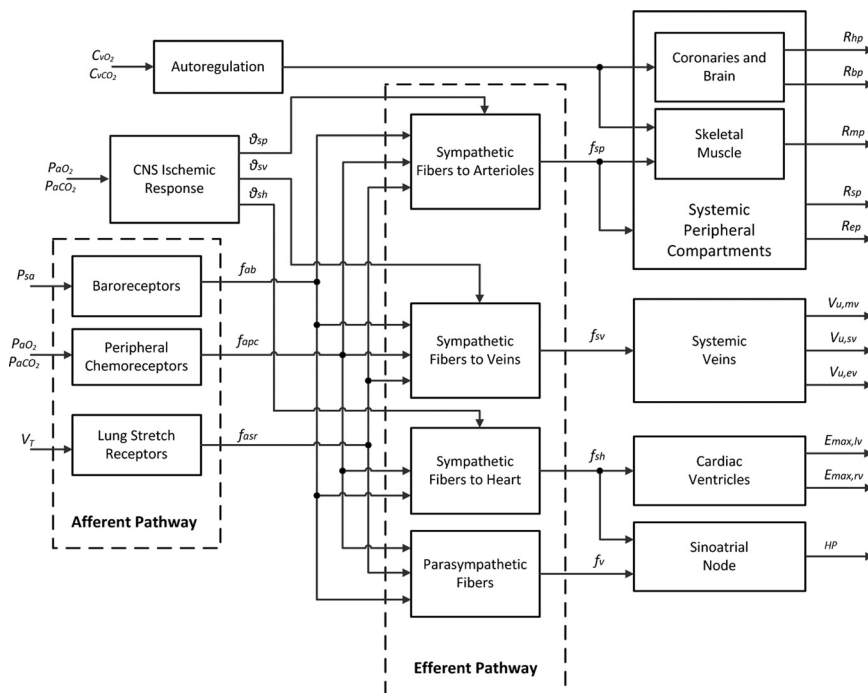


Fig. 10. Schematic block diagram of the cardiovascular control model. P_{sa} , systemic arterial pressure; V_T , tidal volume; f_{ab} , f_{ape} , and f_{asr} , afferent firing frequency of baroreceptors, peripheral chemoreceptors, and lung stretch receptors, respectively; θ_{sp} , θ_{sv} , and θ_{sh} , offset terms representing the effect of the CNS ischemic response on the sympathetic fibers directed to peripheral circulation, veins, and heart, respectively; f_{sp} , f_{sv} , and f_{sh} , activity in the efferent sympathetic fibers directed to the peripheral circulation, the veins, and the heart, respectively; f_v , activity in the vagal efferent fibers; R_{hp} , R_{bp} , R_{mp} , R_{sp} , and R_{ep} , systemic peripheral resistance in coronary, brain, skeletal muscle, splanchnic, and extra-splanchnic vascular beds, respectively; $V_{u,mv}$, $V_{u,sv}$, and $V_{u,ev}$, venous unstressed volume in skeletal muscle, splanchnic, and extra-splanchnic vascular bed, respectively; $E_{max,lv}$ and $E_{max,rv}$, end-systolic elastance of the left and right ventricle, respectively; HP, heart period.

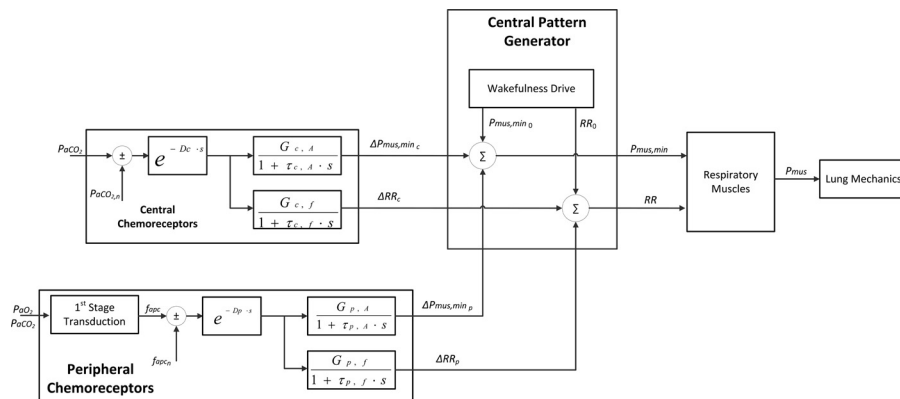


Fig. 11. Schematic block diagram of the respiratory control model. $P_{\text{mus},\min 0}$ and RR_0 , basal values of respiratory muscle pressure amplitude and respiratory rate, respectively; $\Delta P_{\text{mus},\min c}$ and ΔRR_c , variations in respiratory rate and respiratory muscle pressure amplitude induced by the central chemoreceptors; $\Delta P_{\text{mus},\min p}$ and ΔRR_p , variations in respiratory rate and respiratory muscle pressure amplitude induced by the peripheral chemoreceptors; $P_{\text{aCO}_2,\text{n}}$ and $f_{\text{apc},\text{n}}$, nominal value of P_{aCO_2} and f_{apc} , respectively; D_c and D_p , time delay of the central and peripheral chemoreflex mechanisms, respectively; $G_{c,A}$ and $G_{c,f}$, gain factors for the central regulatory mechanism of P_{mus} amplitude and frequency, respectively; $G_{p,A}$ and $G_{p,f}$, gain factors for the peripheral regulatory mechanism of P_{mus} amplitude and frequency, respectively; $\tau_{c,A}$ and $\tau_{c,f}$, time constant of the central regulatory mechanism of P_{mus} amplitude and frequency, respectively; $\tau_{p,A}$ and $\tau_{p,f}$, time constant of the peripheral regulatory mechanism of P_{mus} amplitude and frequency, respectively.

variations of amplitude and frequency of the respiratory muscle generator. The first-stage transduction mechanism obeys the same model of the afferent peripheral chemoreceptor pathway, proposed by Ursino and Magosso (68), which has been used in the cardiovascular control model. This takes into account a multiplicative interaction between O_2 and CO_2 at the peripheral chemoreceptor level, and it has been validated using experimental data from animals under a variety of combined O_2 and CO_2 stimuli. The second stage is described via relationships analogous to those used for the central chemoreceptors (that is, as a first-order dynamic system with a pure delay), the input being the variations in f_{apc} with respect to a set-point value $f_{\text{apc},\text{n}}$.

Parameter Assignment

All of the parameters of the CP Model have been assigned with reference to a 70-kg healthy subject. Most of them are based on previous studies, but some have been modified or newly introduced. They are summarized (see Tables 1–7), along with the corresponding literature references when applicable. In the following sections, the choice of the parameter values for each subsystem will be discussed, with particular emphasis on the new parameters and their modifications with respect to previous studies.

Vascular system. The parameters of the uncontrolled vascular system model have been taken from Ursino and Magosso (44, 69), where detailed justifications about their values can be found. However, some parameters needed to be adjusted or defined to reflect the aforementioned modifications (see Model Development) introduced to the original model structure presented in these previous works, including particularly the following. 1) Resistance and compliance values of the pulmonary peripheral and pulmonary shunt compartments have been assigned to reflect the fact that 1.7% of the total blood flow coming out of the pulmonary arteries (Q_{pa} in Fig. 2) enters the pulmonary shunts, and the remaining 98.3% enters the pulmonary capillaries (33). Furthermore, it has been assumed that the parallel arrangement of pulmonary shunt and pulmonary peripheral compartments provides the equivalent resistance and compliance values as used in Ursino and Magosso (44, 69). 2) The values of the thoracic veins parameters have been given based on Cheng et al. (9) and Neal and Bassingthwaighe (49). 3) As a consequence of the introduction of the thoracic veins compartment, the venous compliance values in all of the parallel systemic districts have been reduced by 30% relative to the values used in Ursino and Magosso (44, 69), so that the total venous compliance is maintained, as suggested in Magosso and Ursino (45). 4) To compensate for the added excess volume, due to

the introduction of the negative P_{pl} , the basal value of the unstressed volume in every vascular compartment within the thoracic cavity has been reduced by 12% relative to the values used in the previous studies (44, 69). 5) The compliance of the overall systemic peripheral circulation has been redistributed among the five parallel districts to guarantee realistic and valid simulation results based on literature. All of the parameters characterizing the uncontrolled vascular system in basal condition (without the action of the regulatory mechanisms) are reported in Tables 1 and 2, along with their corresponding reference source.

Heart. The parameters characterizing the heart model have been given the same value used in previous studies (44, 67, 69). For the sake of brevity, these parameters are not listed here, and the interested reader can refer to the previous studies for the details.

Lung mechanics. The parameters of the lung mechanics model (resistances, compliances, and unstressed volumes of the 4 respiratory mechanics compartments) have been assigned, starting from values reported in Fukui (26) and Rideout (55). However, some adjustments have been made to account for the newly introduced pleural-pressure and chest-wall dynamics and to reproduce realistic, simulated lung volumes, typically observed in normal subjects under quiet breathing conditions, particularly the following. 1) The C_{cw} , not included in Fukui (26) and Rideout (55), has been assigned a value based on van Meurs (71). 2) The amplitude and frequency of the P_{mus} in basal conditions (without the action of the respiratory control model) have been assigned to attain a V_T of ~500 ml and a respiratory rate of 12 breaths/min (72). 3) The initial conditions for the five different pressure nodes in Fig. 6 (state variables) have been assigned, assuming that at time $t = 0$, corresponding to the end-exhalation time, all of the pressures in the lungs equilibrate to P_{atm} , whereas the P_{pl} has a subatmospheric value of -5 cmH₂O (72). 4) The unstressed volume of the alveolar compartment has been modified to produce an end-expiratory lung volume equal to normal functional residual capacity (FRC), based on the following equation

$$V_{A,E} = FRC + C_A \cdot P_{pl,EE} - V_{l,EE} - V_{t,EE} - V_{b,EE} \quad (6)$$

where $P_{pl,EE}$ is the pleural-pressure value at end-exhalation; $V_{l,EE}$, $V_{t,EE}$, and $V_{b,EE}$ represent the end-expiratory volumes of the larynx, trachea, and bronchia, respectively; and FRC is 2.4 liters (72). 5) Finally, the value of τ , governing the exponential expiratory P_{mus} profile, has been assumed to be equal to 1/5 of the expiratory time to allow enough time for lung emptying, and a value of 0.6 has been used for the IE_{ratio} based on the fact that the normal physiological IE_{ratio} is

Table 1. Parameters of the vascular system in basal condition (Eqs. A1–A29 in APPENDIX)

Compliance, ml/mmHg	Unstressed Volume, ml	Resistance, mmHg · s · ml ⁻¹	Inertance, mmHg · s ² · ml ⁻¹
C _{sa} = 0.28 (69)	V _{u,sa} = 0 (69)	R _{sa} = 0.06 (69)	L _{sa} = 0.22 × 10 ⁻³ (69)
C _{sp} = 1.1532 [MODEL]	V _{u,sp} = 274.4 (69)	R _{sp0} = 2.49 (69)	
C _{ep} = 1.0788 [MODEL]	V _{u,ep} = 134.64 (69)	R _{ep0} = 1.655 (69)	
C _{mp} = 0.8184 [MODEL]	V _{u,mp} = 105.8 (69)	R _{mp0} = 2.106 (69)	
C _{hp} = 0.1488 [MODEL]	V _{u,hp} = 24 (69)	R _{hp,n} = 19.71 (69)	
C _{bp} = 0.5208 [MODEL]	V _{u,bp} = 72.13 (69)	R _{bp,n} = 6.6667 (69)	
C _{sv} = 42.777 [MODEL]	V _{u,sv0} = 1435.4 (69)	R _{sv} = 0.038 (69)	
C _{ev} = 14 [MODEL]	V _{u,ev0} = 640.73 (69)	R _{ev} = 0.04 (69)	
C _{mv} = 10.997 [MODEL]	V _{u,mv0} = 503.26 (69)	R _{mv} = 0.05 (69)	
C _{hv} = 2.499 [MODEL]	V _{u,hv} = 98.21 (69)	R _{hv} = 0.224 (69)	
C _{bv} = 7.497 [MODEL]	V _{u,bv} = 294.64 (69)	R _{bv} = 0.075 (69)	
C _{pa} = 0.76 (69)	V _{u,pa} = 0 (69)	R _{pa} = 0.023 (69)	
C _{pp} = 5.7014 [MODEL]	V _{u,pp} = 106.3999 [MODEL]	R _{pp} = 0.0909 [MODEL]	
C _{ps} = 0.0986 [MODEL]	V _{u,ps} = 0 [MODEL]	R _{ps} = 5.2588 [MODEL]	
C _{pv} = 25.37 (69)	V _{u,pv} = 105.6 [MODEL]	R _{pv} = 0.0056 (69)	

See text and Fig. 2 legend for explanation of symbols and subscripts. Note the use of subscripts 0 and n in the unstressed volumes and resistances that are subject to control mechanisms. Total blood volume = 5,300 ml.

between 1:2 and 1:1.5 (52). All of the parameters of the lung mechanics model are reported in Table 3, along with their corresponding reference source when applicable.

Gas exchange and transport. The parameters describing the gas exchange and transport model can be subdivided into parameters pertaining to the lung gas exchange model, to the tissue gas exchange model, and to blood transport, i.e., the two circulatory transport delays τ_{LT} and τ_{VL} (see Fig. 7).

The parameters characterizing the lung gas exchange model can be further divided into three different groups: 1) parameters pertaining to the environmental conditions (e.g., P_{atm} , O_2 and CO_2 gas fractions in air, and saturated water vapor pressure at body temperature), which have been given typical values under the assumption of normal environmental conditions; 2) parameters pertaining to the O_2 and CO_2 dissociation curves, which have been taken from Spencer et al. (60); and 3) parameters pertaining to the physiological status of the subject [percentage of pulmonary shunts (sh) and hemoglobin content (Hgb)], which have been chosen to simulate a 70-kg healthy adult man. The values of the parameters are reported in Table 4 for each group.

As for the tissue gas exchange model, the only parameters involved are the $V_{T,jp}$ and $M_{O_2,jp}$ and $M_{CO_2,jp}$, where j corresponds to the different, combined blood-tissue compartments. The values of $V_{T,jp}$ have been assigned based on literature data, whereas the values of the metabolic rates have been assigned as follows. First, the values of M_{O_2} for the brain, coronary, and skeletal muscle compartments have been taken from Ursino and Magosso (44, 69). Then, the values of M_{O_2} for the splanchnic (sp) and extrasplanchnic (ep) compartments have been given based on the assumption that the total O_2 consumption rate is 250 ml/min (33) and that the ratio $M_{O_2,sp}/M_{O_2,ep}$ is 7.384 (12). Finally, the values of M_{CO_2} for the different compartments have been computed by assuming that the total CO_2 production rate is 210 ml/min (33), corresponding to a respiratory quotient of 0.84, and that the M_{CO_2} ratio between compartment i and compartment j is equal to the corresponding M_{O_2} ratio between the same compartments.

The values of the blood transport delays have been assigned from literature. Some adjustments were made to reflect the fact that part of the circulatory delay has been explicitly taken into account in the venous pool transport model. Particularly, the τ_{LT} has been given the same value used in Lu et al. (42) and Topor et al. (66). As for the τ_{VL} , a value of 10 s has been chosen, considering that a value of 25 s has been used in the model by Lu et al. (42) for the overall tissue-to-lungs delay. This choice is then equivalent to the assumption that a time delay of ~15 s can be attributed to the systemic and the thoracic veins compartments. All of the parameters of the tissue gas exchange model are reported in Table 5, along with the corresponding reference source.

Respiratory control. As we mentioned in Model Development, the majority of the ventilation control models presented in the literature assumes a very simplified structure of the respiratory control system. Hence, assignment of the parameters pertaining to the respiratory control model, based on previous models available in literature, was not always possible. When no reference values were available, the parameters were then calibrated so as to fit experimental data obtained from healthy volunteers under specific respiratory challenges (53, 54).

Referring to Fig. 11, the choice of the respiratory control model parameters is now explained in detail as follows. 1) All of the parameters of the first-stage transduction mechanism in the peripheral chemoreceptor model, equivalent to the model presented by Ursino and Magosso (68), have been maintained to their original values in Ursino and Magosso (68). 2) The values of the central and peripheral chemoreflex time delays (D_c and D_p , respectively), as well as the set-point values for P_{ACO_2} and f_{apc} , have been taken from Magosso and Ursino (44). 3) The two time constants and two gains of the peripheral regulatory mechanism of P_{mus} amplitude and frequency ($\tau_{p,A}$ and $\tau_{p,f}$ and $G_{p,A}$ and $G_{p,f}$, respectively), for which reference values were not available, were calibrated based on the experimental data from isocapnic hypoxia (reduced O_2 with controlled CO_2) experiments, reported by Reynolds and Milhorn (53). These data show the response to a 10-min step input from room air to an 8% O_2 mixture (hypoxia) of a group of 10 healthy male volunteers in terms of V_T , RR, V_e , alveolar O_2 partial pressure (P_{AO_2}), and alveolar CO_2 partial pressure (P_{ACO_2}). During the experiments, P_{ACO_2} was artificially controlled (isocapnia) and kept at a normal physiological value below the chemoreceptor activation threshold. To calibrate the four aforementioned parameters, similar experimental conditions were replicated in the CP Model: the hypoxic stimulus was simulated by imposing a FI_{O_2} step input from 21% (room air) to 8% with the same duration as that one used in the experiments (10 min), whereas the

Table 2. Parameters of the thoracic veins (Eqs. 2 and 3)

Pressure–Volume Relationship	Resistance
D ₁ = 0.3855 mmHg (9)	K _R = 0.001 mmHg · s · ml ⁻¹ (9)
K ₁ = 0.15 mmHg/ml (9)	V _{tv,max} = 350 ml (9)
V _{u,tv} = 130 ml (9)	R _{tv,0} = 0.025 mmHg · s · ml ⁻¹ (9)
D ₂ = -5 mmHg (9)	
K ₂ = 0.4 mmHg (9)	
V _{tv,min} = 50 ml (9)	
K _{xp} = 2 mmHg (49)	
K _{xv} = 8 ml (49)	

See text and references for explanation of symbols.

Table 3. Parameters of the lung mechanics model in basal conditions (Eqs. A30–A41 in APPENDIX)

Compliance, l/cmH ₂ O	Unstressed Volume, ml	Resistance, cmH ₂ O · s · l ⁻¹
C _I = 0.00127 (26)	V _{u,l} = 34.4 (26)	R _{ml} = 1.021 (55)
C _t = 0.00238 (26)	V _{u,t} = 6.63 (26)	R _{lt} = 0.3369 (55)
C _b = 0.0131 (26)	V _{u,b} = 18.7 (26,55)	R _{lb} = 0.3063 (55)
C _A = 0.2 (26)	V _{u,A} = 1.263 [MODEL]	R _{ba} = 0.0817 (55)
Additional Parameters		
C _{cw} = 0.2445 l/cmH ₂ O (71)	FRC = 2.4 liter (72)	P _{pl,EE} = -5 cmH ₂ O (72) P _{mus,min} = -5 cmH ₂ O [MODEL] $\tau = T_E/5$ [MODEL]
RR = 12 breaths/min (72)		
IE _{ratio} = 0.6 [MODEL]		

See text and Fig. 6 legend for explanation of symbols and subscripts. Note the use of subscript 0 for the parameters that are subject to control mechanisms.

isocapnic condition was simulated by including a negative-feedback controller that changed the F_{lCO₂} level dynamically to maintain P_{ACO₂} at its normal range [$\sim 40 \pm 2$ mmHg (14)]. Multiple isocapnic hypoxia simulations were run, starting with default-guessed values of the unknown parameters and using the errors between the model-predicted V_T and RR waveforms and the corresponding experimental data to guide the parameters' fine-tuning. As shown in Fig. 12, the problem of fine tuning the time constants and gains of the peripheral chemoreceptors model can indeed be approached as a typical system-identification problem. The system is excited with a step input F_{lCO₂}, and the responses (V_T and RR) are measured. Due to the isocapnic condition, the central chemoreceptors are not stimulated, and the measured responses are entirely due to the activation of the peripheral chemoreceptors. Hence, the only unknown parameters to be identified are $\tau_{p,A}$ and $\tau_{p,f}$ and G_{p,A} and G_{p,f} in the peripheral chemoreceptors model, whereas all other parameters remain fixed. Note that despite the availability of numerical techniques to solve this specific system-identification problem, the fine-tuning of the model parameters was performed manually, because our goal was only to achieve qualitative agreement between model-simulated and experimental data. In fact, the attempt to obtain a strict quantitative agreement was scientifically irrelevant, due to the large variability of responses existing even among healthy subjects. 4) The two time constants and two gains of the central regulatory mechanism of P_{mus} amplitude and frequency ($\tau_{c,A}$ and $\tau_{c,f}$ and G_{c,A} and G_{c,f}, respectively), for which it was not possible to obtain reference values from literature, were also assigned, following a process similar to the one described above (for the time constants and gains of the peripheral chemoreceptors). In this case, the unknown parameters were calibrated, based on the experimen-

Table 4. Parameters of the lung gas exchange model (Eqs. A42–A56 in APPENDIX)

Environmental Conditions	
F _{lO₂} = 21.0379%	P _{atm} = 760 mmHg
F _{lCO₂} = 0.0421%	P _{ws} = 47 mmHg
K = 1.2103	
Dissociation Curves (60)	
C _{sat,O₂} = 9 mmol/l	C _{sat,CO₂} = 86.11 mmol/l
h ₁ = 0.3836	h ₂ = 1.819
α_1 = 0.03198 mmHg ⁻¹	α_2 = 0.05591 mmHg ⁻¹
β_1 = 0.008275 mmHg ⁻¹	β_2 = 0.03255 mmHg ⁻¹
K ₁ = 14.99 mmHg	K ₂ = 194.4 mmHg
Physiological Status	
sh = 1.7 (33)	Hgb = 15 g/dl (72)

See Fig. 8 legend for explanation of symbols.

Table 5. Parameters of the tissue gas exchange model (Eqs. A57–A78 in APPENDIX)

Compartment	Tissue Volume, ml	O ₂ Consumption Rate, ml/min	CO ₂ Production Rate, ml/min
Coronaries	284 (40)	24 (44,69)	20.16 [MODEL]
Brain	1,300 (70)	47.502 (44,69)	39.9017 [MODEL]
Skeletal muscles	31,200 (59)	51.6 (44,69)	43.344 [MODEL]
Splanchnic	2,673 (4,28,57)	108.419 [MODEL]	91.0720 [MODEL]
Extrapsplanchnic	262 (56)	14.683 [MODEL]	12.3337 [MODEL]
Blood Transport Delays			
τ_{LT} = 18 s (42,66)	τ_{TVL} = 10 s [MODEL]		

tal data reported by Reynolds et al. (54), related to hypercapnic conditions (increased CO₂). The data contain the average respiratory responses (time profiles of V_T, RR, V_e, P_{AO₂}, and P_{ACO₂}) observed across 14 subjects, after a 25-min hypercapnic step input from normal room air to 7% CO₂. Similarly to what is described above, to assign the unknown parameters, the experimental conditions were first simulated in the CP Model, starting with guessed default values for $\tau_{c,A}$, $\tau_{c,f}$, G_{c,A}, and G_{c,f}. Then, an iterative calibration process was performed, where the errors between model outputs (V_T and RR) and experimental data were used to guide parameter fine-tuning. Throughout this process, the parameters of the peripheral chemoreceptors model were fixed to the values found in the previous calibration step. Again, the problem of fine tuning the parameters is seen as a typical system-identification problem (see Fig. 13), where the system is excited with a known step input F_{lCO₂}, and the responses (V_T and RR) are measured. Note that in this case, unlike the isocapnic hypoxia case above, where only the peripheral chemoreceptors were activated, the V_T and RR responses are determined by contributions from both the central and peripheral chemoreflex mechanisms. However, since the parameters of the peripheral chemoreceptors model were maintained fixed throughout the calibration process, it was still possible to isolate the contribution from the central chemoreceptors and identify the parameters that allow a good fitting of the model outputs to the experimental results. Note that even in this case, during the parameter-adjustment process, only qualitative agreement between model predictions and experimental data was sought, and no attempt to minimize the corresponding error via numerical techniques was made.

All of the parameters of the respiratory control model are provided in Table 6, along with the corresponding reference source when applicable. The results from the hypercapnia and isocapnic hypoxia simulations, obtained via the parameter calibration procedures described above, are included in the companion paper (8).

Cardiovascular control. Since the cardiovascular control model is formally equivalent to the models by Ursino and Magosso (44, 69), except for the afferent peripheral chemoreceptors pathway that is based on Ursino and Magosso (68), all of its parameters have been taken from these previous models (44, 68, 69). However, some of the parameters related to the autoregulation mechanism and the balance of the afferent information from the different receptors, operated at the level of the ANS, have been modified with respect to their original values presented in Ursino and Magosso (44, 69). This was necessary to reproduce the typical cardiovascular response to hypercapnia and hypoxia observed in the healthy population and reported in the literature (1, 38, 47, 62). In fact, simulations of hypercapnia and hypoxia, using the nominal parameter values reported in Ursino and Magosso (44, 69), produced cardiovascular responses that were not in agreement with the experimental data reported in the literature, particularly in terms of HR and ABP changes. Hence, a sensitivity

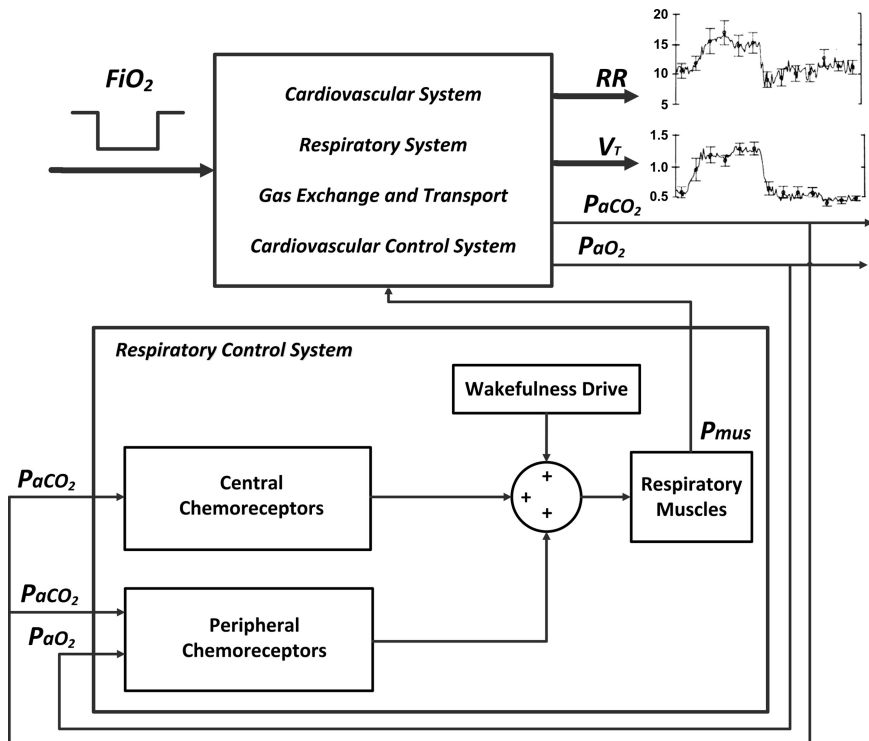


Fig. 12. Block diagram summarizing the calibration procedure used to assign the values of the time constants and gains of the peripheral chemoreceptor model. The system is excited with a step input [fraction of inspired O₂ (F_{iO_2})], and the response (V_T and RR) is measured.

analysis (SA) of the impact of model parameters on cardiovascular outputs during hypercapnia and hypoxia was conducted to assess which parameters contributed the most to the above-mentioned discrepancies between model-predicted and experimental responses. Particularly, the parameters of the cardiovascular control model were ranked, based on the local sensitivity matrix, according to the procedure suggested by Ellwein et al. (22).

As a result of this SA, 11 parameters were identified as the most sensitive, and their values were modified compared with their initial values proposed in Ursino and Magosso (44, 69). Here, for the sake of brevity, the details of the SA procedure are not reported, and only the values of the modified parameters are listed in Table 7. The interested reader can refer to previous publications (44, 68, 69) for a list of the additional, unchanged parameters. The comparison

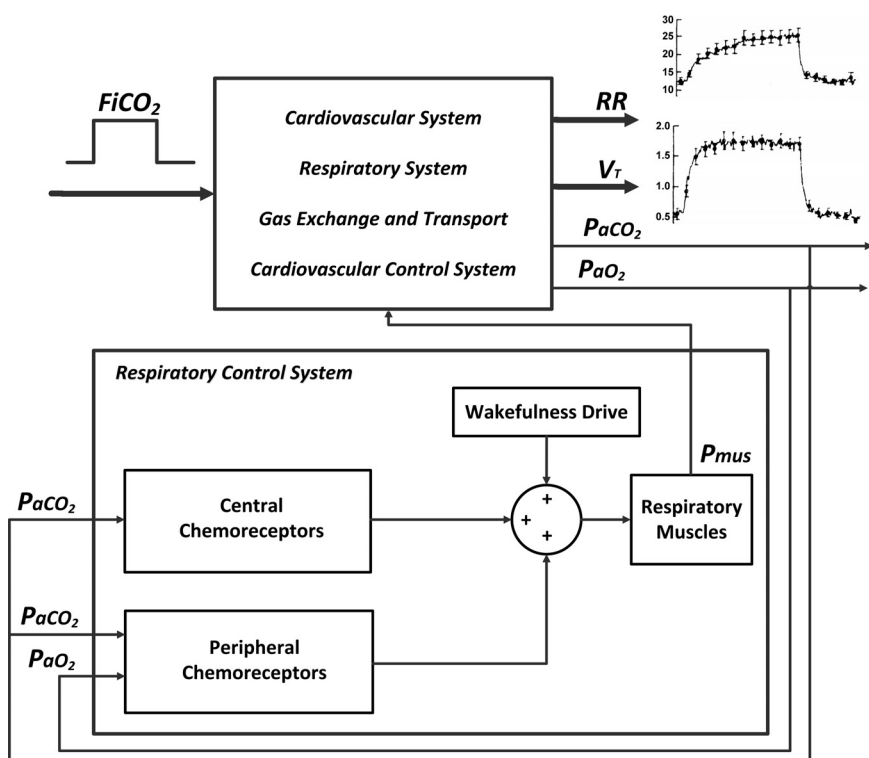


Fig. 13. Block diagram summarizing the calibration procedure used to assign the values of the time constants and gains of the central chemoreceptor model. The system is excited with a step input [fraction of inspired CO₂ (F_{iCO_2})], and the response (V_T and RR) is measured.

Table 6. Parameters of the respiratory control model (Eqs. A79–A84 in APPENDIX)

Peripheral Chemoreceptors		
$D_p = 7 \text{ s}$ (44)	$G_{p,A} = 1,310 \text{ cmH}_2\text{O}/v$ [MODEL]	$G_{p,f} = 0.8735 \text{ breaths} \cdot \text{min}^{-1} \cdot v^{-1}$ [MODEL]
$\tau_{p,A} = 83 \text{ s}$ [MODEL]	$\tau_{p,f} = 147.78 \text{ s}$ [MODEL]	$f_{apc,n} = 3.7 \text{ spikes/s}$ (44)
Central Chemoreceptors		
$D_c = 8 \text{ s}$ (44)	$G_{c,A} = 850 \text{ cmH}_2\text{O/mmHg}$ [MODEL]	$G_{c,f} = 0.9 \text{ breaths} \cdot \text{min}^{-1} \cdot \text{mmHg}^{-1}$ [MODEL]
$\tau_{c,A} = 105 \text{ s}$ [MODEL]	$\tau_{c,f} = 400 \text{ s}$ [MODEL]	$P_{aCO_2,n} = 40 \text{ mmHg}$ (44)

v , spikes/s. See Fig. 11 legend for explanation of symbols.

between model-simulated responses to hypoxia and hypercapnia with the experimental counterparts is shown in the companion paper (8).

RESULTS

The combined model has 78 differential equations, >70 algebraic equations, and 240 parameters associated with its components. Table 8 shows the distribution of the state variables, model parameters, and main outputs of this integrated CP Model. The model was programmed in Matlab-Simulink (MathWorks, Natick, MA), and the numerical integration of the differential equations was performed using the fourth-order Runge-Kutta method with fixed-step size.

A reasonable reproduction of variables typically observed on a generally healthy adult population is the basis for further applications of our integrated CP Model. To verify the ability of the present model in these regards, we analyze the model's predicted outputs in normal resting conditions, and we present a comparison with waveforms or average values typically observed in humans. Particularly, our analysis includes the model behavior, both in terms of mean values, i.e., averaged values over a respiratory or cardiac cycle, and intracycle (respiratory or cardiac cycle) values. In presenting the results, major emphasis is put on the new aspects of the model compared with previous work (44, 69). All model results are based on 1,000 s simulations using the parameter values reported in Tables 1–7.

Hemodynamics

Table 9 summarizes the static values of the relevant clinical hemodynamic variables that the CP model generates and compares them with values typically measured on healthy humans in normal resting conditions. The table shows that the model-predicted outputs are within normal physiological ranges of the general population.

Figure 14 shows a representative, simulated left-ventricle PV loop, along with the pressure and volume time profiles over an entire cardiac cycle. The model is thus able to capture the typical features of a realistic PV loop, both in terms of shape and amplitude. For the specific cardiac cycle shown in the figure, the left-ventricular volume ranged from 132 ml (end-diastolic volume) to 53 ml (end-systolic volume), providing a stroke volume of 79 ml and an ejection fraction of 79/132, or 59%. Note that these values slightly change from one cardiac cycle to the next because of variations of P_{pl} and the effects of cardiovascular control mechanisms that induce cyclic changes in HR, ventricular contractility, and afterload.

Figure 15 compares model-generated left- and right-ventricular output flows with experimental waveforms (42). Both the

amplitude and duration of the simulated flow waveforms resemble the experimental data. The left-ventricular flow has a higher peak value and shorter time duration compared with the right-ventricular flow. For the specific cardiac cycle shown in Fig. 15, the left-ventricle peak flow is 688.5 ml/s, and the right-ventricle peak flow is 484.5 ml/s; the left-ventricle ejection phase lasts for 0.192 s, whereas the right-ventricle ejection phase lasts for 0.252 s. This is due to the greater contractility and higher afterload of the left ventricle compared with the right. Numerical integration of the flow waveforms over the entire cardiac cycle gives the values of left- and right-ventricular stroke volume as 79.21 and 79.32 ml, respectively. Hence, despite the dissimilarities in amplitude and time duration, the areas enclosed by the two waveforms are essentially the same.

Respiratory Mechanics

Figure 16 shows the pressure and flow waveforms generated by the lung mechanics model in normal resting conditions when the chemoreceptors are silent, and RR and $P_{mus,min}$ are equal to their basal values. At the beginning of inspiration, alveolar pressure equals P_{atm} , i.e., zero pressure. During inspiration, the negative P_{mus} drives pleural pressure to decrease from its resting value of -5 to approximately -8 cmH₂O, which in turn, decreases alveolar pressure below atmospheric value and allows air to flow into the mouth, trachea, bronchea, and alveoli. At the end of inspiration, when the respiratory muscles start relaxing, pleural pressure returns to its baseline value, and alveolar pressure becomes slightly positive, allowing air to flow out of the lung. The V_T produced by the model is ~540 ml, 40 ml of which is spent in ventilating the dead space and the remaining flowing into the alveoli to participate to gas exchange (see Fig. 16). This is in agreement with normal physiological behavior under quiet breathing conditions (72).

Table 7. Parameters of the cardiovascular control model modified with respect to Ursino and Magosso (44,69)

Afferent Lung Stretch Receptors Pathway		
$G_{asr} = 11.76 \text{ spikes} \cdot l^{-1} \cdot s^{-1}$		
Efferent Sympathetic Pathway		
$W_{b,sp} = -1.1375$	$W_{pc,sp} = 1.716$	$W_{sr,sp} = -0.3997$
$W_{b,sv} = -1.0806$	$W_{pc,sv} = 1.716$	$W_{sr,sv} = -0.2907$
$W_{b,sh} = -1.75$		
Autoregulation		
$g_{b,O_2} = 140 \text{ ml blood/ml O}_2$	$g_{h,O_2} = 490 \text{ ml blood/ml O}_2$	$g_{m,O_2} = 420 \text{ ml blood/ml O}_2$

See Ursino and Magosso (44,69) for explanation of symbols.

Table 8. Number of state variables, parameters, and outputs in the combined cardiopulmonary model

	State Variables	Parameters	Outputs
Cardiovascular system	17	74	43
Respiratory system	5	19	8
Gas exchange and transport	26	29	9
Cardiovascular control	26	104	8
Respiratory control	4	14	2

Figure 17 compares a model-simulated airflow waveform during a typical breathing cycle with an experimental tracing from a normal subject. As evident from Fig. 17A, the simulated inspiratory flow pattern has the typical dome shape that has been reported in the literature (51), with the peak flow reached early in the inspiratory part of the cycle. However, some discrepancies between simulated and experimental data can be observed in terms of time and amplitude of the maximum and minimum peak flow. These discrepancies could be ascribed to the high intrasubject variability in the respiratory patterns and as shown in Fig. 17B, can be reduced via slight modifications of some of the parameters of the respiratory muscle pressure model (e.g., $P_{\text{mus},\text{min}0}$, IE_{ratio} , and τ).

Figure 18 shows the comparison between a model-simulated pleural-pressure waveform and an experimental tracing of P_{pl} from a dog during spontaneous breathing conditions. Again, even though some discrepancies can be observed in terms of timing and amplitude of pleural-pressure swings, Fig. 18 shows that the model-simulated P_{pl} dynamics resemble those observed *in vivo*.

Gas Exchange and Transport

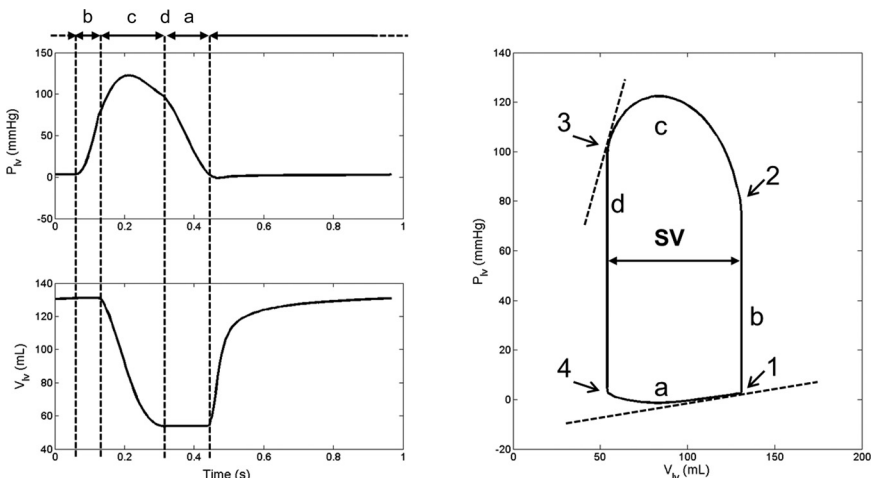
The main outputs of the gas exchange and transport model are summarized in Table 10, in terms of their mean values over one respiratory cycle and compared with typical values in resting healthy humans. Furthermore, in Figs. 19–22, the time profiles of partial pressures at different levels throughout the cardiopulmonary system are shown. Particularly, Fig. 19 shows the variation of PaO_2 and PaCO_2 , along with the lung volume waveform. PaO_2 and PaCO_2 are relatively constant and oscillate around their mean values, 98.9 and 39.55 mmHg, respectively (see Table 10), in synchrony with the respiratory cycle. PaO_2 varies from 96.93 to 100.8 mmHg, and it increases during inhalation and decreases during exhalation. The opposite is valid for PaCO_2 , which oscillates between 37.89 and 41.06 mmHg. The mean values of the simulated PaO_2 and PaCO_2 waveforms are in agreement with the values typically observed in healthy humans from arterial blood gas analysis during normal resting conditions (see Table 10). Comparison of model-generated PaO_2 and PaCO_2 fluctuations with corresponding human data is more difficult to obtain, due to the lack of continuous PaO_2 and PaCO_2 measurements available in the literature. However, PaO_2 fluctuations of $\pm 1\text{--}4$ mmHg, in synchrony with the respiratory cycle and in the same direction as those generated by the model, have been reported in animal studies performed on cats and lambs. Furthermore, the magnitudes of the model-generated fluctuations agree with those reported in previous simulation studies (24, 39). It is worth noticing that cardiogenic oscillations are present in the simulated PaO_2 and PaCO_2 profiles, a phenomenon that has been

reported by previous investigators as well (24, 26). This is essentially due to the coupling between the tidal respiratory model and the pulsatile cardiovascular model, which is an essential feature of our integrative modeling approach. Figure 20 shows the variations of blood gas composition in the venous section in terms of partial pressure. Variations of partial pressure of O_2 and CO_2 in the mixed venous blood (PvO_2 and PvCO_2 , respectively), such as those in PaO_2 and PaCO_2 , are affected by the respiratory cycle events, but the effects of blood pulsatility are less evident, due to the filtering introduced by the venous circulation. The mean values of PvO_2 and PvCO_2 are also in the typical ranges observed in normal resting subjects (see Table 10). Figure 21 shows the comparison between model-simulated PAO_2 and PACO_2 waveforms and their expected physiological counterparts, as shown in physiology textbooks (14, 26). Clearly, the dynamics predicted by the model are different from their physiological counterparts. For instance, the simulated waveforms contain higher-frequency dynamics that can be attributed to cardiogenic events, in addition to lower-frequency variations that are related to the respiratory events. This generates the appearance, in the simulated PO_2 and PCO_2 waveforms, of plateau phases superimposed to monotonic fall and rise periods in synchrony with the respiratory events. In contrast, the physiological counterparts do not contain the aforementioned higher-frequency dynamics, as the effects of blood pulsatility are typically ignored in traditional physiology textbooks. Nevertheless, the overall trend of the simulated PO_2 and PCO_2 waveforms, with respect to the respiratory cycle events, is in agreement with the expected behavior reported in the literature. Particularly, at the beginning of the inspiratory phase, PACO_2 rises to a maximum, and PAO_2 drops to a minimum; this represents the period during which dead-space air is entering the alveoli. This is followed by a period of rapidly increasing PO_2 and falling PCO_2 , which reflects the effects of the introduction of fresh, inspired air into the alveoli. The maximum PO_2 and minimum PCO_2 are reached toward the end of the inspiratory phase, when maximum dilution with fresh air has been achieved. During the expiratory phase, the partial-pressure variations change direction, with PO_2 progressively

Table 9. Static values of main hemodynamic variables

Variable	Model Simulation	Normal Range
Arterial pressure, mmHg		
Mean	90.74	70–105 (21a)
Systolic	122.79	90–140 (34)
Diastolic	78.86	60–90 (34)
Vena Cava Pressure, mmHg		
Systolic	3.79	2–14 (34)
Diastolic	2.72	0–8 (34)
Right Atrium Pressure, mmHg		
Mean	0.7	2–6 (21a)
Right-Ventricle Pressure, mmHg		
Systolic	24.45	15–28 (34)
Diastolic	-1.2	0–8 (34)
Pulmonary Artery Pressure, mmHg		
Systolic	24.41	15–28 (34)
Diastolic	7.38	5–16 (34)
Left Atrium Pressure, mmHg		
Mean	4	2–6 (21a)
Left-Ventricle Pressure, mmHg		
Systolic	122.79	90–140 (34)
End-diastolic	0.2	4–12 (34)

Fig. 14. Left-ventricle pressure and volume outputs. *Left:* time patterns of left-ventricle pressure (P_{lv} ; *top*) and volume (V_{lv} ; *bottom*). Dotted lines mark the 4 cardiac phases: *a*, filling phase; *b*, isometric contraction phase; *c*, ejection phase; *d*, isometric relaxation phase. *Right:* PV loop of the left ventricle. The 4 cardiac phases (*a*, *b*, *c*, and *d*) are shown, along with the stroke volume (SV) and the opening and closing points of the heart valves: 1, mitral valve closing point; 2, aortic valve opening point; 3, aortic valve closing point; 4, mitral valve opening point. The 2 dotted lines tangent to the PV loop at points 1 and 3 represent the diastolic and the end-systolic PV functions, respectively.



falling and PCO_2 progressively rising. This reflects the effects of continued gas exchange during a period when no fresh air is supplied to the alveoli.

Finally, Fig. 22 shows a comparison between the model-generated, dead-space PCO_2 and a typical time-based capnographic waveform obtained in normal adult patients over a single respiratory cycle (63). The simulated dead-space PCO_2 resembles the capnogram in terms of both shape and amplitude, even though some minor differences can be observed. First, the baseline in the simulated dead-space PCO_2 tracing is

slightly above zero (see Table 10), whereas the normal capnogram has a zero-baseline value. Second, during the inhalation phase, the capnographic waveform suddenly reaches the zero-baseline value and remains flat until early exhalation; this is not the case for the simulated dead-space PCO_2 waveform, probably because the capnographic waveform is obtained by sampling the airflow at the mouth, whereas the simulated PCO_2 waveform is representative of a lumped dead-space compartment that is between the atmospheric air and the internal alveolar compartments.

Heart–Lung Interactions

As mentioned in INTRODUCTION, heart–lung interactions take a variety of forms. Mechanical interactions are one of these forms and are mainly due to the effects of intrathoracic pressure on VR and cardiac function. During inhalation, VR increases, due to the decreasing P_{pl} that produces a shift in blood volume from the systemic to the pulmonary circulation. The variations in VR are associated with variations in cardiac performance: the increased VR during inhalation improves right-ventricular filling and preload, thus generating an increase in right-ventricular output flow and stroke volume, according to the Frank–Starling mechanism. The effects of inspiration on the left ventricle are in the opposite direction: the decreasing P_{pl} affects the pulmonary vasculature, which acts as a capacitance reservoir that holds more blood so that left-ventricular filling is reduced with the consequent drop in left-ventricular output flow and stroke volume via the Frank–Starling mechanism. The situation is reversed during expiration, when P_{pl} gradually returns to baseline. In this case, VR and right-ventricular output flow are reduced, whereas more blood is forced from the pulmonary vasculature into the left heart, and hence, left-ventricular output flow is increased. The variations of intrathoracic pressure associated with the respiratory events also have effects on systemic arterial pressure. Systolic, diastolic, and pulse arterial pressures are lowest during inspiration and highest at the peak of expiration. These variations result partially from transmission of intrathoracic pressure to the ascending and thoracic aorta and partially from the respiratory-related changes in left-ventricular output flow (58), discussed above. Reductions in systolic blood pressure during inhalation of 4–5 mmHg have been reported in the

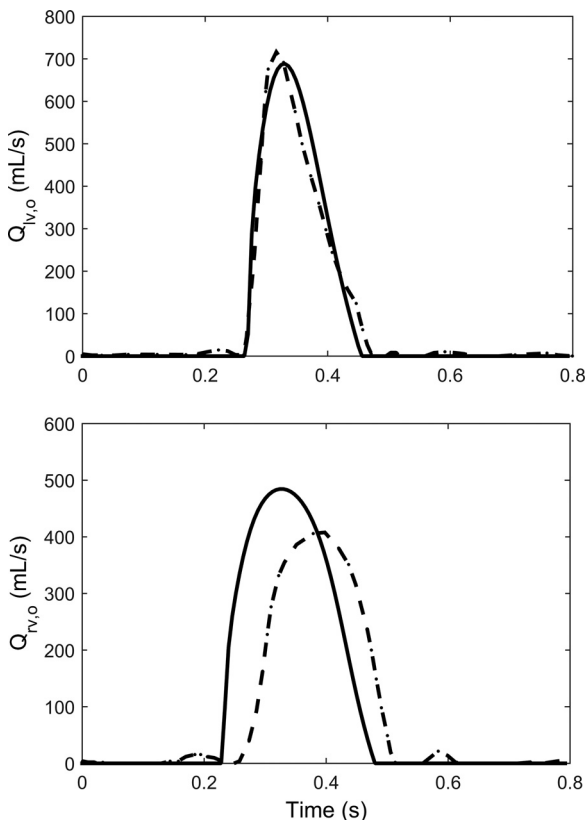


Fig. 15. Model-predicted flows (continuous line) compared with reported experimental data (dotted line). *Top:* left-ventricle output flow ($Q_{lv,o}$). *Bottom:* right-ventricle output flow ($Q_{rv,o}$). The experimental data have been redrawn from Fig. 7 of Lu et al. (42).

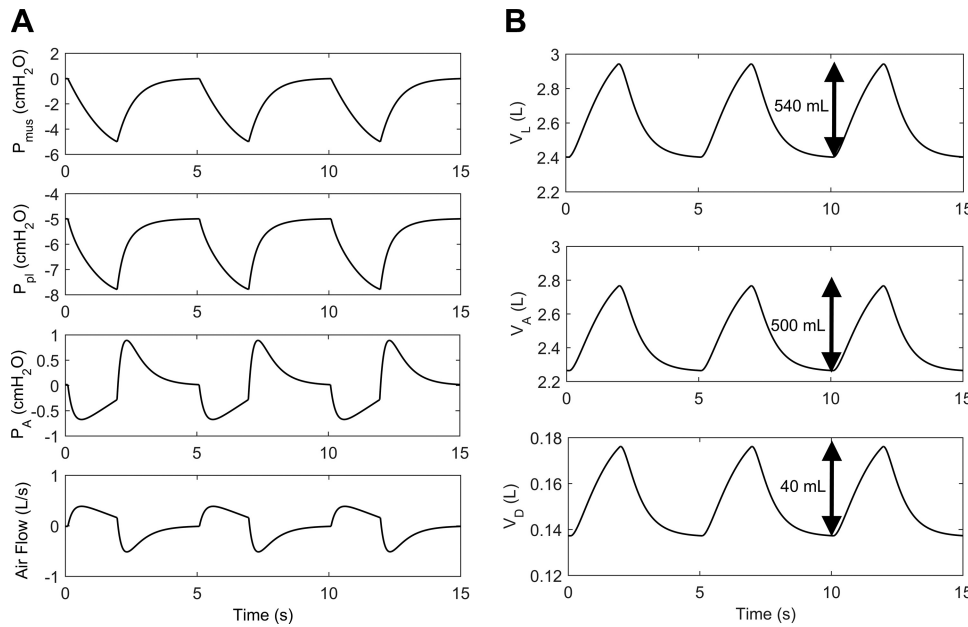


Fig. 16. Pressure, volume, and flow waveforms generated by the lung mechanics model. A, top to bottom: P_{mus} , P_{pl} , alveolar pressure (P_{A}), and airflow. B, top to bottom: lung volume (V_L), V_A , and V_D .

literature (58), and variations of >5 mmHg are considered signs of pathological conditions and are commonly referred to as “pulsus paradoxus” (48).

The present model is able to account for such mechanical interactions between heart and lungs, thanks to the inclusion of the P_{pl} as the reference external pressure for the vascular compartments that lie within the thoracic cavity (see Model Development). Figure 23 shows the simulated time profiles of VR (computed in the model as the instantaneous flow entering the right atrium), left- and right-ventricular output flow, and stroke volume, along with the pleural-pressure waveform over few representative respiratory cycles. The model-predicted hemodynamic changes driven by respiratory events are qualitatively in agreement with the physiological mechanisms described above: VR and right-ventricular stroke volume rise during inspiration and fall during exhalation, whereas left-ventricular stroke volume variations have the opposite direction. The model predicts an inspiratory rise in right-ventricular

stroke volume of ~ 7 ml, which agrees well with the expected variations in normal condition [5 ml, according to Ruskin et al. (58)]. On the other hand, the model-predicted changes in left-ventricular stroke volume are slightly underestimated: only 1.16 ml inspiratory falls with respect to the end-exhalation value. The effects of respiration are visible in the systemic arterial blood pressure waveform (P_{sa}) as well, as shown in Fig. 24, where the systolic and diastolic P_{sa} values are plotted together with the pleural-pressure waveform over a few consecutive respiratory cycles. The model-predicted changes in systolic and diastolic blood pressure are qualitatively in agreement with the expected behavior: systolic and diastolic blood pressure drops during inhalation and rises during exhalation. However, even in this case, the model-predicted variations are smaller than what is typically observed in normal subjects: 0.7 mmHg model-predicted reduction in systolic blood pressure, corresponding to $\sim 0.5\%$ of the end-exhalation value compared with 4 mmHg and 3% variation in normal subjects (58).

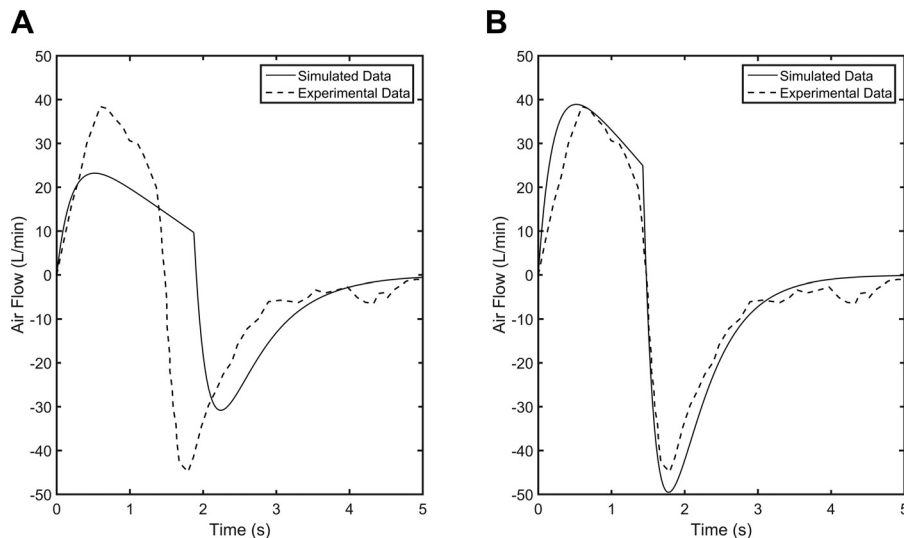


Fig. 17. Comparison between simulated and experimental airflow waveforms. Pneumotachogram from a normal subject showing patterns of flow in quiet mouth breathing (dashed lines); reproduced from Proctor (51). Model-generated airflow (continuous lines). A: simulated data obtained using the nominal parameter values reported in Table 3. B: simulated data obtained after modifying the parameters $P_{\text{mus},\text{mino}}$, inspiratory-expiratory time ratio, and τ in the P_{mus} model.

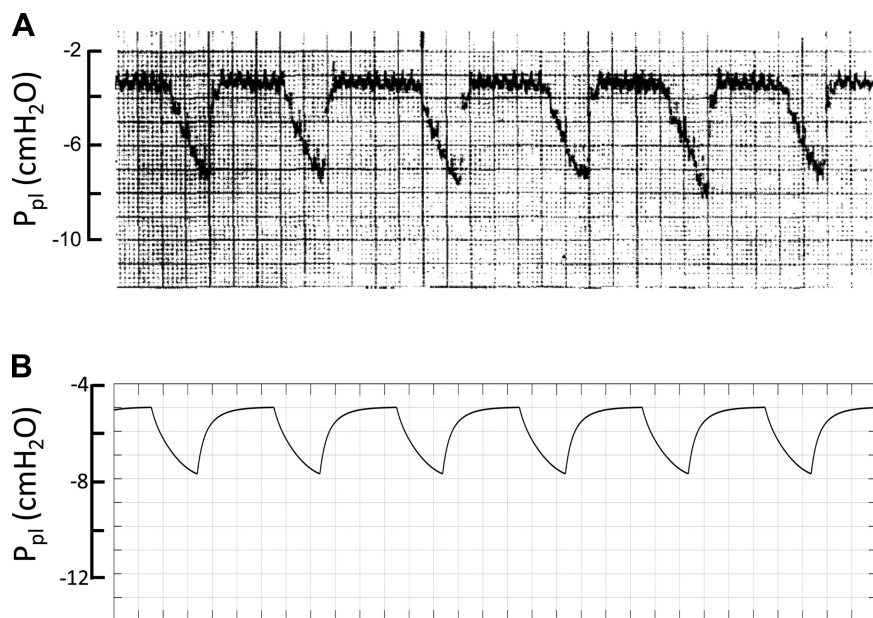


Fig. 18. Comparison between simulated and experimental pleural-pressure waveforms. *A*: tracing of pleural pressure from a dog in a supine position during spontaneous breathing; reproduced with permission from D'Angelo and Agostoni (16). *B*: model-generated pleural-pressure waveform. Note that the time division in *A* and *B* is 1 s, and the scales have been adjusted to allow for visual comparison.

Possible reasons for such discrepancy between model results and experimental observations will be explained in DISCUSSION, and these aspects might be the subject of future study.

Another well-known physiological mechanism of cardiorespiratory interactions is the respiratory sinus arrhythmia (RSA), which is a naturally occurring variation in HR, in synchrony with the respiratory cycle, whereby HR increases during inhalation and decreases during exhalation. The model, in its present form and with its nominal parameter values, is able to reproduce RSA partially by capturing only certain aspects of the phenomenon. Particularly, the model-simulated HR does vary within a respiratory cycle, but the magnitude of the variations (0.8 beat/min) is underestimated compared with what is typically observed in normal subjects under resting conditions (~5 beats/min). Furthermore, the timing of the model-simulated HR variations is slightly out of phase with respect to the respiratory events, resulting in HR decrease during inhalation rather than an increase. Manipulations of some model parameters (e.g., reduction of the RR_0) have shown to be effective in improving both the amplitude and the timing mismatches, with slight effects on the model-simulated respiratory and gas exchange variables (moderate PaO_2 increase and $PaCO_2$ decrease with respect to their normal baseline values). Due to the preliminary nature of these results, we have decided not to cover these aspects in the present paper and leave the RSA topic as the subject of future investigations, as will be mentioned in DISCUSSION.

DISCUSSION

This paper presents an integrated mathematical model of the cardiovascular and respiratory systems and their interactions. It comprises the following physiological systems and mechanisms: heart (4 chambers), systemic circulation (arteries—5 peripheral and 5 venous compartments), pulmonary circulation (arteries, vessels, veins, and shunt), lung mechanics (larynx, trachea, bronchi, alveoli, pleural cavity, and diaphragmatic muscle), thoracic cavity, ANS (sympathetic and vagal), local autoregulation, CNS ischemic response, as well as gas ex-

change (lung and tissue), including Bohr and Haldane effects. It is the fruit of a multiyear effort and is presented in two papers: the present paper describes the model development and verification under normal physiological conditions, whereas the companion paper (8) describes the response under hypercapnic and hypoxic conditions. The model contains close to 150 equations, divided almost equally between ordinary differential and algebraic equations. The results suggest good fidelity between the model's output and published human data in normophysiological (see Figs. 15, 17, 18, 21, and 22 and Tables 9 and 10), as well as hypercapnic and hypoxic conditions (companion paper). There are close to 70 state variables that can be outputted or observed from the model (such as pressures, flows, and gas concentrations) and ~240 parameters that represent physical properties and geometry of the anatomy (such as alveolar compliance, bronchial resistance, left-ventricular elastance, and systemic vascular resistance).

To facilitate its use, the model has been coupled with a stand-alone Graphical User Interface. This allows the user to interact directly with the model via a web application (<http://cardiopulmonarymodel.com/>).

The main aspects that deserve a discussion are the integrative nature of the model and the potential benefits of its future applications for the physiological/clinical community.

Table 10. Mean values of main gas composition variables

Variable	Model Simulation	Normal Value
Arterial PO_2 , mmHg	98.9	100 (14)
Arterial PCO_2 , mmHg	39.55	40 (14)
Mixed venous PO_2 , mmHg	42.3	40 (14)
Mixed venous PCO_2 , mmHg	43.5	46 (14)
Mixed venous CO_2 , ml/dl	15.11	15 (21a)
Mixed venous C_{CO_2} , ml/dl	52.07	53 (5)
Alveolar PO_2 , mmHg	100.7	104 (14)
Alveolar PCO_2 , mmHg	39.5	40 (14)
Dead space PO_2 , mmHg	148.5*	149.2* (14)
Dead space PCO_2 , mmHg	1.47*	0.3* (14)

*Dead-space PO_2 and PCO_2 values are maximum and minimum values obtained within a respiratory cycle, respectively.

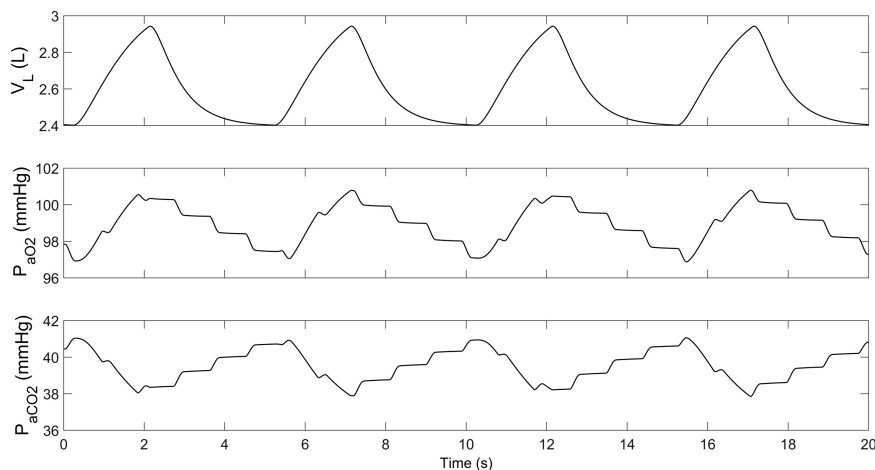


Fig. 19. Time profiles of model-generated arterial O_2 and CO_2 partial pressures. Top to bottom: V_L , P_{ao_2} , and P_{aco_2} .

Most previous models focused on a single aspect of the overall cardiorespiratory system (such as respiratory mechanics, cardiovascular regulation, or ventilation control). The main objective of the present work is to combine these partial descriptions and allow the cardiorespiratory dynamics to ensue from an integrated model, consisting of many subsystems that are mixed and continuously influence each other in a multi-feedback, multiscale arrangement. This fully integrative perspective will unfold more of the richness and complexity of the cardiovascular system. A possible concern is that the model contains too many parameters (~ 240) to be really fitted to any individual subject. This criticism is certainly correct. However, we think that tailoring the model to individual cases does not require all parameters to be fine-tuned but only those that are crucial to the specific physiological aspects under investigation. For instance, if the objective of a study is to investigate individual variability in ventilation, then only parameters characterizing respiratory mechanics and ventilation control can be tuned. The model can simulate individual variations in these aspects and then can furnish indications on how a change in respiratory mechanics and ventilation is reflected in the other parts of the model (cardiac, metabolic, hemodynamical, etc.) still assumed in the prototypical configuration.

The present model has many potential applications. First, it can be used as an educational tool, to illustrate and explain the complexity of the cardiorespiratory relationships and the pos-

sible consequences of specific parameter changes. To this regard, the high number of parameters constitutes an advantage rather than a limitation of the model, providing a more complete illustration of many aspects at the anatomical, physiological, and functional level.

Second, the model can be used as a research tool to elucidate the physiological reasons for the variability of cardiorespiratory quantities observed across different individuals in a healthy condition. For instance, with the assumption that some parameters can vary within a physiological range in healthy individuals, the model can produce a range of physiological waveforms for each different parameter set. In other words, model complexity can be exploited to explain this intrinsic “irregularity” of the healthy condition, a crucial aspect in physiology and clinics, which often lacks a rigorous scientific characterization.

Another important application of the model is the analysis of cardiorespiratory responses to acute perturbations (posture change, metabolic alteration, hemorrhage, change in air gas content, etc.). In fact, one function of feedback regulatory mechanisms (that represent an essential part of the present model) is to cope with acute changes of the internal or external environment to regulate vital and metabolic functions. An example will be illustrated in the second companion paper (8), devoted to a thorough investigation of the model response to hypoxia and hypercapnia.

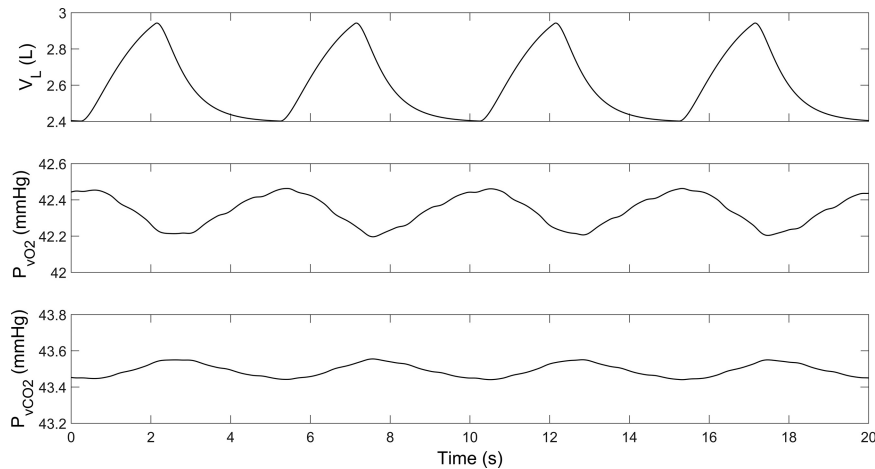


Fig. 20. Time profiles of model-generated mixed venous O_2 and CO_2 partial pressures. Top to bottom: V_L , partial pressure of O_2 in mixed venous blood (P_{vo_2}), and partial pressure of CO_2 in mixed venous blood (P_{vco_2}).

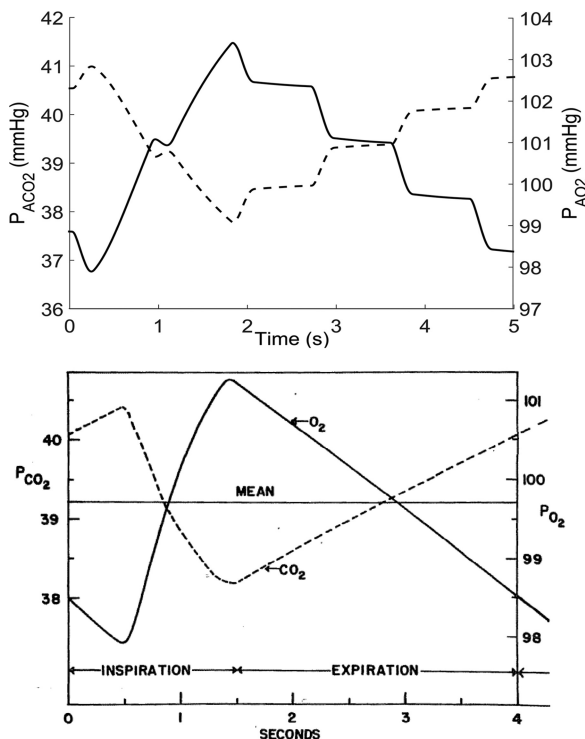


Fig. 21. Time profiles of O_2 and CO_2 partial pressures in the alveolar space during a respiratory cycle. *Top*: model simulations; PAO_2 , alveolar O_2 partial pressure; $PACO_2$, alveolar CO_2 partial pressure. *Bottom*: expected behavior from literature (14, 26).

Finally, an important future use of the model is to simulate and analyze cardiorespiratory pathologies. This aspect, however, requires future validation studies. In the present paper and in the companion, we have not investigated pathological conditions: all simulations were performed using a single parameter set, representing a generic, healthy individual. Hence, we have no present validation on disease states. Nevertheless, we

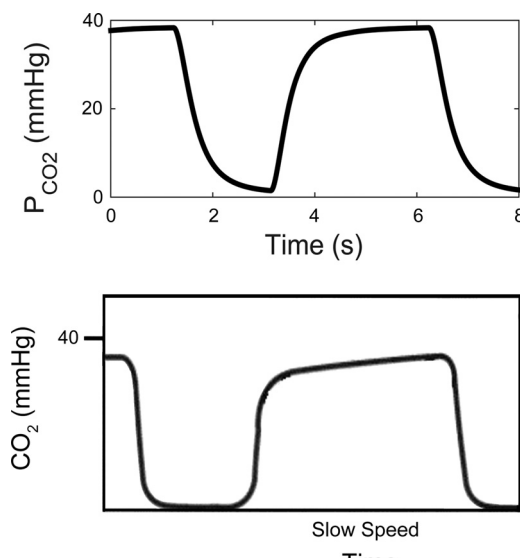


Fig. 22. Comparison between model-generated PCO_2 in the dead space (*top*) and a representative normal time-based capnogram (*bottom*); reproduced with permission from Thompson and Jaffe (63).

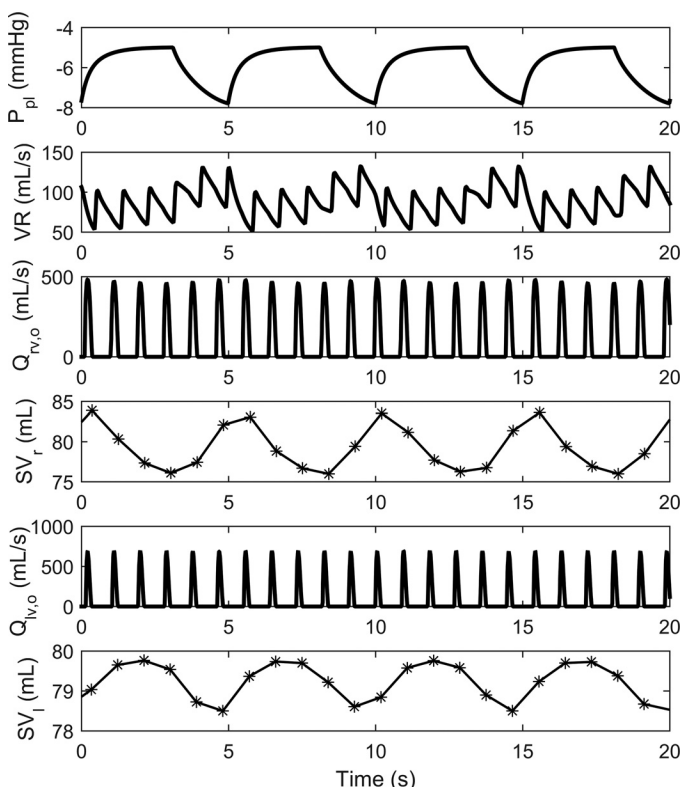


Fig. 23. Mechanical effects of respiration on cardiovascular function. *Top to bottom*: time profiles of P_{pl} , venous return (VR), $Q_{rv,o}$, right-ventricular stroke volume (SV_r), $Q_{lv,o}$, and left-ventricular stroke volume (SV_l).

claim that the model has the potential to investigate pathological conditions, thanks to two important features. First, we incorporated a multitude of physiological mechanisms in a single theoretical setting, providing a more complete description than any previous comparable model. Second, all model parameters have a clear physiological/functional meaning. This may allow the description of pathologies to be implemented on the basis of a true physiological knowledge in an effort to reproduce where and how a disease affects the cardiopulmonary system. All of these aspects can have enormous impacts, both in education programs and, in perspective, in helping clinical reasoning. Application of the model to the simulation of diseases will require the following: 1) understanding which parameters potentially may be affected by the pathology; 2) testing the effect of these parameter changes in the model; and 3) comparing the modified model waveforms with data available from clinical measurements.

Once the model has been used to simulate a specific pathology, it may then be used to simulate therapeutic interventions, which on the other hand, can only be simulated if the appropriate therapy has an input path to one of the submodels. For instance, a mechanical ventilator has a direct path to the lung mechanics submodel.

Finally, if enough knowledge is not available to characterize a pathology fully in terms of mechanisms involved and parameter values, then the model may be used as a reverse engineering tool. For instance, one can try to identify which parameter changes produce derangements of vital quantities, in agreement with clinical observations, and generate new physiological hypotheses about the origins of a specific pathology.

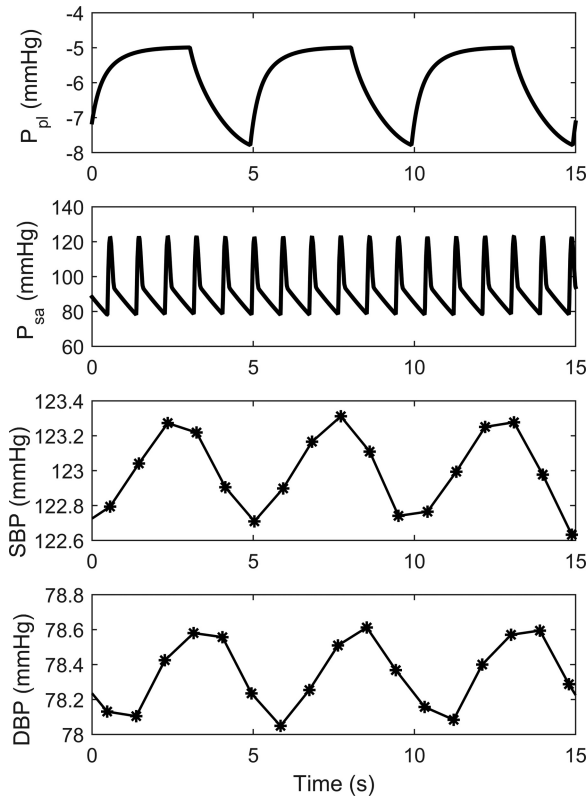


Fig. 24. Mechanical effects of respiration on systemic arterial pressure. *Top to bottom:* time profiles of P_{pl} , P_{sa} , systolic blood pressure (SBP), and diastolic blood pressure (DBP).

Now that we have described the salient characteristics of the model, it is equally important to discuss its main limitations. These limitations, discussed below, will be targets of future improvements.

First, the model does not include several organs and regulatory mechanisms that affect the cardiopulmonary system, particularly the following. 1) It does not possess a kidney, and no fluid balance is computed; we have not included equations for fluid exchange at the capillaries under hydraulic and oncotic pressure gradients. Hence, the blood volume is constant, and the only way to modify it is via a hemorrhagic shock. 2) The model focuses on short-term regulation and hence, does not include long-term control mechanisms, such as the renin-angiotensin-aldosterone system. 3) The metabolism module is limited to constant metabolic rates of the different organs and does not include acid-base balance. 4) There is no thermoregulation, and no thermal or humidity factors affect the lungs.

In addition, as pointed out in RESULTS, the effects of respiration on arterial blood pressure and left-ventricular stroke volume are slightly underestimated. This discrepancy may be due to the fact that the present model does not account for ventricular interdependence via the septum, which may play an important role in explaining the reduced left-ventricular stroke volume during inhalation. The left and right ventricles, in fact, share a common pericardial space and are separated by a mobile intraventricular septum. When the right-ventricular diastolic volume increases during inhalation, the septum tends to shift to the left, reducing left-ventricular compliance and causing a further reduction in stroke volume (25). Another

reason for the underestimated effects of respiration on systemic arterial pressure may be related to the fact that the lumped systemic arterial compartment in the model is not subject to P_{pl} , whereas in reality, the ascending and the thoracic aorta are within the thoracic cavity and hence, are directly affected by P_{pl} variations. Further expansion of the model to address these limitations specifically is envisioned.

Finally, the model is unable to reproduce fully the physiological RSA phenomenon (see RESULTS). To this regard, it is worth mentioning that the physiological origins of RSA are still arguments of debate in the physiological community. The two current competing theories are the following: 1) RSA is the result of baroreflex-mediated variations in HR, triggered by the blood pressure fluctuations associated with the respiratory events (21), and 2) RSA is a centrally mediated mechanism independent of baroreflex activation (21). Thus if the central origin theory were confirmed, then the discrepancy between model-simulated RSA and the corresponding physiological observations, pointed out in RESULTS, might be justified, since the present model does not include such mechanism and hence, would certainly not be able to account for it. On the other hand, if the baroreflex was solely responsible for the origin of RSA, then in principle, the model should be able to reproduce RSA correctly. Hence, justification of the aforementioned discrepancy would be more challenging. These, along with the effects of parameter modifications (e.g., RR_0) on the simulated RSA, will be the topic of further investigation and future model development.

In conclusion, we have developed a novel, integrated cardiopulmonary model. The level of rigor included in each submodel reflects current available knowledge. The authors' hope is to contribute to the understanding of our cardiopulmonary system in a deterministic way so that we can better quantify our physiological knowledge and ultimately make more informed clinical decisions, leading to a better quality of life.

APPENDIX

In the following section, a quantitative description of the model is provided. Only equations concerning the new aspects of the model and the modifications introduced with respect to the previous models, upon which the present one is built, are presented. They describe the circulatory system, lung mechanics, lung gas exchange, tissue gas exchange, venous pool gas transport, and respiratory control.

The Circulatory System

The equations describing the circulatory system have been obtained by enforcing conservation of mass and balance of forces for each vascular compartment in Fig. 2.

Systemic circulation.

$$C_{sa} \cdot \frac{dP_{sa}}{dt} = Q_{lv,o} - Q_{sa} \quad (A1)$$

$$L_{sa} \cdot \frac{dQ_{sa}}{dt} = P_{sa} - P_{ep} - R_{sa} \cdot Q_{sa} \quad (A2)$$

$$V_{sa} = C_{sa} \cdot P_{sa} + V_{u,sa} \quad (A3)$$

$$C_{p,ep} \cdot \frac{dP_{ep}}{dt} = Q_{sa} - \sum_j Q_{jp} \quad (A4)$$

$$P_{ep} = P_{sp} = P_{mp} = P_{bp} = P_{hp} \quad (A5)$$

$$Q_{jp} = \begin{cases} \frac{P_{jp} - P_{jv}}{R_{jp}} & P_{jp} \geq P_{jv} \\ 0 & P_{jp} < P_{jv} \end{cases} \quad (A6)$$

$$V_{jp} = C_{jp} \cdot P_{jp} + V_{u,jp} \quad (A7)$$

$$C_{sv} \cdot \frac{dP_{sv}}{dt} + \frac{dV_{u,sv}}{dt} = Q_{sp} - Q_{sv} \quad (A8)$$

$$C_{mv} \cdot \frac{dP_{mv}}{dt} + \frac{dV_{u,mv}}{dt} = Q_{mp} - Q_{mv} \quad (A9)$$

$$C_{hv} \cdot \frac{dP_{hv}}{dt} = Q_{hp} - Q_{hv} \quad (A10)$$

$$C_{bv} \cdot \frac{dP_{bv}}{dt} = Q_{bp} - Q_{bv} \quad (A11)$$

$$\begin{aligned} P_{ev} = \frac{1}{C_{ev}} \cdot [V_{tot} - V_{sa} - V_{hp} - V_{bp} - V_{mp} - V_{sp} - V_{ep} - V_{hv} - V_{bv} \\ - V_{mv} - V_{sv} - V_{tv} - V_{ra} - V_{rv} - V_{hv} - V_{bv} - V_{mv} - V_{sv} \\ - V_{tv} - V_{ra} - V_{rv} - V_{pa} - V_{pp} - V_{ps} - V_{pv} - V_{la} \\ - V_{lv} - V_{u,ev}] \quad (A12) \end{aligned}$$

$$Q_{jv} = \begin{cases} \frac{P_{jv} - P_{tv}}{R_{jv}} & P_{jv} \geq P_{tv} \\ 0 & P_{jv} < P_{tv} \end{cases} \quad (A13)$$

$$V_{jv} = C_{jv} \cdot P_{jv} + V_{u,jv} \quad (A14)$$

$$\frac{dV_{tv}}{dt} = \sum_j Q_{jv} - Q_{tv} \quad (A15)$$

$$Q_{tv} = \frac{P_{tv} - P_{ra}}{R_{tv}} \quad (A16)$$

$$P_{tv} = P_{pl} + P_{tm,tv} \quad (A17)$$

where $j = e, s, m, b, h$ indicates the specific systemic compartment; $C_{pe,q} = \sum_j C_{jp}$ is the equivalent peripheral compliance given by the parallel arrangement of the five different systemic peripheral compartments; and $P_{tm,tv}$ is given by Eq. 2 (see Model Development). Note that for the extrasplanchnic systemic veins pressure (P_{ev}), the conservation of mass equation has been replaced by an algebraic compatibility equation (Eq. A12) to guarantee that the total volume of blood (V_{tot}) contained in the cardiovascular system is constant at any time during the simulations.

Pulmonary circulation.

$$C_{pa} \cdot \frac{d(P_{pa} - P_{pl})}{dt} = Q_{rv,o} - Q_{pa} \quad (A18)$$

$$L_{pa} \cdot \frac{dQ_{pa}}{dt} = P_{pa} - P_{pp} - R_{pa} \cdot Q_{pa} \quad (A19)$$

$$V_{pa} = C_{pa} \cdot (P_{pa} - P_{pl}) + V_{u,pa} \quad (A20)$$

$$(C_{ps} + C_{pp}) \cdot \frac{d(P_{pp} - P_{pl})}{dt} = Q_{pa} - Q_{ps} - Q_{pp} \quad (A21)$$

$$Q_{pp} = \frac{P_{pp} - P_{pv}}{R_{pp}} \quad (A22)$$

$$Q_{ps} = \frac{P_{ps} - P_{pv}}{R_{ps}} \quad (A23)$$

$$P_{ps} = P_{pp} \quad (A24)$$

$$V_{pp} = C_{pp} \cdot (P_{pp} - P_{pt}) + V_{u,pp} \quad (A25)$$

$$V_{ps} = C_{ps} \cdot (P_{ps} - P_{pl}) + V_{u,ps} \quad (A26)$$

$$C_{pv} \cdot \frac{d(P_{pv} - P_{pl})}{dt} = Q_{pp} + Q_{ps} - Q_{pv} \quad (A27)$$

$$Q_{pv} = \frac{P_{pv} - P_{la}}{R_{pv}} \quad (A28)$$

$$V_{pv} = C_{pv} \cdot (P_{pv} - P_{pl}) + V_{u,pv} \quad (A29)$$

The Heart

The equations describing the heart model are formally equivalent to those reported in Ursino and Magosso (44, 69), but modifications have been introduced to account for the presence of intrathoracic pressure.

The Lung Mechanics

The equations describing the lung mechanics model have been obtained by applying conservation of mass to the electrical analog shown in Fig. 6

$$C_l \cdot \frac{dP_l}{dt} = \frac{P_{ao} - P_l}{R_{ml}} - \frac{P_l - P_{tr}}{R_{lt}} \quad (A30)$$

$$C_{tr} \cdot \frac{d(P_{tr} - P_{pl})}{dt} = \frac{P_l - P_{tr}}{R_{lt}} - \frac{P_{tr} - P_b}{R_{tb}} \quad (A31)$$

$$C_b \cdot \frac{d(P_b - P_{pl})}{dt} = \frac{P_{tr} - P_b}{R_{tb}} - \frac{P_b - P_A}{R_{ba}} \quad (A32)$$

$$C_A \cdot \frac{d(P_A - P_{pl})}{dt} = \frac{P_b - P_A}{R_{ba}} \quad (A33)$$

$$C_{CW} \cdot \frac{d(P_{pl} - P_{mus})}{dt} = \frac{P_l - P_{tr}}{R_{lt}} \quad (A34)$$

$$\dot{V} = \frac{P_{ao} - P_l}{R_{ml}} \quad (A35)$$

$$\dot{V}_A = \frac{P_b - P_A}{R_{ba}} \quad (A36)$$

$$V_l = C_l \cdot P_l + V_{u,l} \quad (A37)$$

$$V_{tr} = C_{tr} \cdot (P_{tr} - P_{pl}) + V_{u,tr} \quad (A38)$$

$$V_b = C_b \cdot (P_b - P_{pl}) + V_{u,b} \quad (A39)$$

$$V_A = C_A \cdot (P_A - P_{pl}) + V_{u,A} \quad (A40)$$

$$V_D = V_l + V_{tr} + V_b \quad (A41)$$

The equations describing the profile of the P_{mus} have been provided in Model Development (see Eq. 4).

Lung Gas Exchange

$$\begin{aligned} V_D \cdot \frac{dF_{D,O2}}{dt} = u(\dot{V}) \cdot \dot{V} \cdot (F_{I,O2} - F_{D,O2}) \\ + u(-\dot{V}) \cdot \dot{V}_A \cdot (F_{D,O2} - F_{A,O2}) \end{aligned} \quad (A42)$$

$$\begin{aligned} V_D \cdot \frac{dF_{D,CO2}}{dt} = u(\dot{V}) \cdot \dot{V} \cdot (F_{I,CO2} - F_{D,CO2}) \\ + u(-\dot{V}) \cdot \dot{V}_A \cdot (F_{D,CO2} - F_{A,CO2}) \end{aligned} \quad (A43)$$

$$\begin{aligned} V_A \cdot \frac{dF_{A,O2}}{dt} = u(\dot{V}) \cdot \dot{V}_A \cdot (F_{D,O2} - F_{A,O2}) \\ - K \cdot \left(Q_{pa} \cdot (1 - sh) \cdot (C_{pp,O2} - \tilde{C}_{v,O2}) + V_{PP} \frac{dC_{pp,O2}}{dt} \right) \end{aligned} \quad (A44)$$

$$V_A \cdot \frac{dF_{A,CO2}}{dt} = u(\dot{V}) \cdot \dot{V}_A \cdot (F_{D,CO2} - F_{A,CO2}) \\ - K \cdot \left(Q_{pa} \cdot (1 - sh) \cdot (C_{pp,CO2} - \bar{C}_{v,CO2}) + V_{pp} \frac{dC_{pp,CO2}}{dt} \right) \quad (A45)$$

$$C_{pp,O2} = C_{sat,O2} \cdot \frac{(X_{pp,O2})^{\frac{1}{h_1}}}{1 + (X_{pp,O2})^{\frac{1}{h_1}}} \quad (A46)$$

$$X_{pp,O2} = P_{pp,O2} \cdot \frac{1 + \beta_1 \cdot P_{pp,CO2}}{K_1 \cdot (1 + \alpha_1 \cdot P_{pp,CO2})} \quad (A47)$$

$$C_{pp,CO2} = C_{sat,CO2} \cdot \frac{(X_{pp,CO2})^{\frac{1}{h_2}}}{1 + (X_{pp,CO2})^{\frac{1}{h_2}}} \quad (A48)$$

$$X_{pp,CO2} = P_{pp,CO2} \cdot \frac{1 + \beta_2 \cdot P_{pp,O2}}{K_2 \cdot (1 + \alpha_2 \cdot P_{pp,O2})} \quad (A49)$$

$$P_{pp,O2} = P_{A,O2} \quad (A50)$$

$$P_{pp,CO2} = P_{A,CO2} \quad (A51)$$

$$P_{A,O2} = F_{A,O2} \cdot (P_{atm} - P_{ws}) \quad (A52)$$

$$P_{A,CO2} = F_{A,CO2} \cdot (P_{atm} - P_{ws}) \quad (A53)$$

$$C_{a,O2} = \frac{Q_{pp} \cdot C_{pp,O2} + Q_{ps} \cdot \bar{C}_{v,O2}}{Q_{pp} + Q_{ps}} \quad (A54)$$

$$C_{a,CO2} = \frac{Q_{pp} \cdot C_{pp,CO2} + Q_{ps} \cdot \bar{C}_{v,CO2}}{Q_{pp} + Q_{ps}} \quad (A55)$$

$$S_{a,O2}\% = \frac{C_{a,O2} - P_{a,O2} \cdot 0.003/100}{Hgb \cdot 1.34} \cdot 100 \quad (A56)$$

where Eqs. A42–A45 are derived based on conservation of mass principles, Eqs. A46–A49 are the dissociation functions, as reported in Spencer et al. (60), Eqs. A50 and A51 represent the instantaneous equilibrium assumption between alveolar space and capillary blood, Eqs. A52 and A53 relate gas fractions in the lungs to their corresponding partial pressures, Eqs. A54 and A55 represent the mixing between capillary and shunted blood, and Eq. A56 is used to compute O₂ saturation in the arterial blood.

Note: u is the Heaviside step function, and it is introduced to make Eqs. A42–A45 valid, both during inhalation and exhalation; K is a proportionality constant that allows conversion of volumes from body temperature pressure saturated to standard temperature pressure dry conditions; 1.34 in Eq. A56 is the O₂ capacity (expressed in milliliters O₂/g Hgb), and 0.003/100 represents the solubility of O₂ in blood (expressed in milliliters O₂/ml blood/mmHg).

Tissue Gas Exchange

The complete equations describing the tissue gas exchange model are the following

$$(V_{T,hp} + V_{hp}) \cdot \frac{dC_{hp,O2}}{dt} = Q_{hp,in} \cdot (\bar{C}_{a,O2} - C_{hp,O2}) \\ - M_{O2,hp} \quad (A57)$$

$$(V_{T,hp} + V_{hp}) \cdot \frac{dC_{hp,CO2}}{dt} = Q_{hp,in} \cdot (\bar{C}_{a,CO2} - C_{hp,CO2}) \\ + M_{CO2,hp} \quad (A58)$$

$$(V_{T,bp} + V_{bp}) \cdot \frac{dC_{bp,O2}}{dt} = Q_{bp,in} \cdot (\bar{C}_{a,O2} - C_{bp,O2}) \\ - M_{O2,bp} \quad (A59)$$

$$(V_{T,bp} + V_{bp}) \cdot \frac{dC_{bp,CO2}}{dt} = Q_{bp,in} \cdot (\bar{C}_{a,CO2} - C_{bp,CO2}) \\ + M_{CO2,bp} \quad (A60)$$

$$(V_{T,mp} + V_{mp}) \cdot \frac{dC_{mp,O2}}{dt} = Q_{mp,in} \cdot (\bar{C}_{a,O2} - C_{mp,O2}) \\ - M_{O2,mp} \quad (A61)$$

$$(V_{T,mp} + V_{mp}) \cdot \frac{dC_{mp,CO2}}{dt} = Q_{mp,in} \cdot (\bar{C}_{a,CO2} - C_{mp,CO2}) \\ + M_{CO2,mp} \quad (A62)$$

$$(V_{T,ep} + V_{ep}) \cdot \frac{dC_{ep,O2}}{dt} = Q_{ep,in} \cdot (\bar{C}_{a,O2} - C_{ep,O2}) \\ - M_{O2,ep} \quad (A63)$$

$$(V_{T,ep} + V_{ep}) \cdot \frac{dC_{ep,CO2}}{dt} = Q_{ep,in} \cdot (\bar{C}_{a,CO2} - C_{ep,CO2}) \\ + M_{CO2,ep} \quad (A64)$$

$$(V_{T,sp} + V_{sp}) \cdot \frac{dC_{sp,O2}}{dt} = Q_{sp,in} \cdot (\bar{C}_{a,O2} - C_{sp,O2}) \\ - M_{O2,sp} \quad (A65)$$

$$(V_{T,sp} + V_{sp}) \cdot \frac{dC_{sp,CO2}}{dt} = Q_{sp,in} \cdot (\bar{C}_{a,CO2} - C_{sp,CO2}) \\ + M_{CO2,sp} \quad (A66)$$

where Q_{j,p,in} is the blood flow entering the jth peripheral compartment (see Fig. 9 legend for further definition of subscripts).

Venous Pool Gas Transport

$$V_{hv} \cdot \frac{dC_{hv,O2}}{dt} = Q_{hp} \cdot (C_{hp,O2} - C_{hv,O2}) \quad (A67)$$

$$V_{hv} \cdot \frac{dC_{hv,CO2}}{dt} = Q_{hp} \cdot (C_{hp,CO2} - C_{hv,CO2}) \quad (A68)$$

$$V_{bv} \cdot \frac{dC_{bv,O2}}{dt} = Q_{bp} \cdot (C_{bp,O2} - C_{bv,O2}) \quad (A69)$$

$$V_{bv} \cdot \frac{dC_{bv,CO2}}{dt} = Q_{bp} \cdot (C_{bp,CO2} - C_{bv,CO2}) \quad (A70)$$

$$V_{mv} \cdot \frac{dC_{mv,O2}}{dt} = Q_{mp} \cdot (C_{mp,O2} - C_{mv,O2}) \quad (A71)$$

$$V_{mv} \cdot \frac{dC_{mv,CO2}}{dt} = Q_{mp} \cdot (C_{mp,CO2} - C_{mv,CO2}) \quad (A72)$$

$$V_{ev} \cdot \frac{dC_{ev,O2}}{dt} = Q_{ep} \cdot (C_{ep,O2} - C_{ev,O2}) \quad (A73)$$

$$V_{ev} \cdot \frac{dC_{ev,CO2}}{dt} = Q_{ep} \cdot (C_{ep,CO2} - C_{ev,CO2}) \quad (A74)$$

$$V_{sv} \cdot \frac{dC_{sv,O2}}{dt} = Q_{sp} \cdot (C_{sp,O2} - C_{sv,O2}) \quad (A75)$$

$$V_{sv} \cdot \frac{dC_{sv,CO2}}{dt} = Q_{sp} \cdot (C_{sp,CO2} - C_{sv,CO2}) \quad (A76)$$

$$\begin{aligned} V_{tv} \cdot \frac{dC_{v,O2}}{dt} = & Q_{hv} \cdot (C_{hv,O2} - C_{v,O2}) + Q_{bv} \cdot (C_{bv,O2} - C_{v,O2}) \\ & + Q_{mv} \cdot (C_{mv,O2} - C_{v,O2}) + Q_{ev} \cdot (C_{ev,O2} - C_{v,O2}) \\ & + Q_{sv} \cdot (C_{sv,O2} - C_{v,O2}) \end{aligned} \quad (A77)$$

$$\begin{aligned} V_{tv} \cdot \frac{dC_{v,CO2}}{dt} = & Q_{hv} \cdot (C_{hv,CO2} - C_{v,CO2}) + Q_{bv} \cdot (C_{bv,CO2} - C_{v,CO2}) \\ & + Q_{mv} \cdot (C_{mv,CO2} - C_{v,CO2}) + Q_{ev} \cdot (C_{ev,CO2} - C_{v,CO2}) \\ & + Q_{sv} \cdot (C_{sv,CO2} - C_{v,CO2}) \end{aligned} \quad (A78)$$

Respiratory Control

The respiratory control model affects the respiratory system via modifications in the amplitude ($P_{mus,min}$) and the frequency (RR) of the P_{mus} (see Fig. 11), according to

$$P_{mus,min} = P_{mus,min0} + \Delta P_{mus,min}c + \Delta P_{mus,min}p \quad (A79)$$

$$RR = RR_0 + \Delta RR_c + \Delta RR_p \quad (A80)$$

where $P_{mus,min0}$ is the basal value of the respiratory muscle pressure amplitude, RR_0 is the basal value of the respiratory muscle pressure frequency, ΔRR_c and $\Delta P_{mus,min}c$ are the variations in respiratory rate and respiratory muscle pressure amplitude induced by the central chemoreceptors, and ΔRR_p and $\Delta P_{mus,min}p$ are the variations in respiratory rate and respiratory muscle pressure amplitude induced by the peripheral chemoreceptors.

The central chemoreceptor mechanism has been described as a first-order dynamic system, whose input-output relationships are governed by the following equations (2)

$$\frac{d\Delta P_{mus,min}c}{dt} = \frac{-\Delta P_{mus,min}c + G_{c,A} \cdot u_c}{\tau_{c,A}} \quad (A81)$$

$$\frac{d\Delta RR_c}{dt} = \frac{-\Delta RR_c + G_{cf} \cdot u_c}{\tau_{cf}} \quad (A82)$$

$$\text{with } u_c(t) = P_{aCO_2}(t - D_c) - P_{aCO_2,n}$$

where D_c is a delay that accounts for the time it takes for blood to travel from the systemic arteries to the central chemosensitive area in the brain; $G_{c,f}$ and $G_{c,A}$ are the gains of the P_{mus} amplitude and frequency control mechanisms, respectively; $\tau_{c,f}$ and $\tau_{c,A}$ are the corresponding time constants; and $P_{aCO_2,n}$ is the PaO_2 set-point value.

The peripheral chemoreceptor mechanism has been described as a two-stage transduction mechanism (see Model Development). The first stage has been taken from previous work (68), where complete equations are provided. The second stage has been described similarly to the central mechanism as the first-order dynamic system (2), as below

$$\frac{d\Delta P_{mus,min}p}{dt} = \frac{-\Delta P_{mus,min}p + G_{p,A} \cdot u_p}{\tau_{p,A}} \quad (A83)$$

$$\frac{d\Delta RR_p}{dt} = \frac{-\Delta RR_p + G_{p,f} \cdot u_p}{\tau_{p,f}} \quad (A84)$$

$$\text{with } u_p(t) = f_{acp}(t - D_p) - f_{acp,n}$$

where D_p is a delay that accounts for the time it takes for blood to travel from the systemic arteries to the peripheral chemosensitive area; $G_{p,f}$ and $G_{p,A}$ are the gains of the P_{mus} amplitude and frequency control mechanisms, respectively; $\tau_{p,f}$ and $\tau_{p,A}$ are the corresponding time constants; and $f_{acp,n}$ is the afferent peripheral chemoreceptor activity set-point value.

Cardiovascular Control

The equations describing the cardiovascular control model are taken from Ursino and Magosso (44, 69). The only modification is in the description of the afferent peripheral chemoreceptor mechanism, as described in Model Development.

DISCLOSURES

No conflicts of interest, financial or otherwise, are declared by the authors.

AUTHOR CONTRIBUTIONS

Author contributions: A.A., L.C., M.U., and N.W.C. conception and design of research; A.A. and L.C. performed experiments; A.A. and L.C. analyzed data; A.A., L.C., and N.W.C. interpreted results of experiments; A.A. prepared figures; A.A. and N.W.C. drafted manuscript; A.A., L.C., M.U., and N.W.C. edited and revised manuscript; A.A., L.C., M.U., and N.W.C. approved final version of manuscript.

REFERENCES

1. Ainslie PN, Poulin MJ. Ventilatory, cerebrovascular, and cardiovascular interactions in acute hypoxia: regulation by carbon dioxide. *J Appl Physiol* 97: 149–159, 2004.
2. Albanese A, Chbat NW, Ursino M. Transient respiratory response to hypercapnia: analysis via a cardiopulmonary simulation model. In: *33rd Annual International Conference of the IEEE Engineering in Medicine and Biology Society*. Boston, MA: Boston Marriott Copley Place Hotel, 2011.
3. Andersen V, Sonne J, Sletting S, Prip A. The volume of the liver in patients correlates to body weight and alcohol consumption. *Alcohol Alcohol* 35: 531–532, 2000.
4. Arthurs GJ, Sudhakar M. Carbon dioxide transport. *Cont Educ Anaesth Crit Care Pain* 5: 207–210, 2005.
5. Athanasiades A, Ghorbel F, Clark JW, Nirajan SC, Olansen JB, Zwischenberger JB, Bidani A. Energy analysis of a nonlinear model of the normal human lung. *J Biol Syst* 8: 115–139, 2000.
6. Chbat NW, Giannessi M, Albanese A, Ursino M. A comprehensive cardiopulmonary simulation model for the analysis of hypercapnic respiratory failure. In: *31st Annual International Conference of the IEEE Engineering in Medicine and Biology Society*. Minneapolis, MN: The Hilton Minneapolis, 2009.
7. Cheng L, Albanese A, Ursino M, Chbat NW. An integrated mathematical model of the human cardiopulmonary system: model validation under hypercapnia and hypoxia. *Am J Physiol Heart Circ Physiol*. 310: 2016. doi:10.1152/ajpheart.00923.2014.
8. Cheng L, Ivanova O, Fan HH, Khoo MC. An integrative model of respiratory and cardiovascular control in sleep-disordered breathing. *Respir Physiol Neurobiol* 174: 4–28, 2010.
9. Cheng L, Khoo MC. Modeling the autonomic and metabolic effects of obstructive sleep apnea: a simulation study. *Front Physiol* 2: 111, 2012.
10. Chiari L, Avanzolini G, Ursino M. A comprehensive simulator of the human respiratory system: validation with experimental and simulated data. *Ann Biomed Eng* 25: 985–99, 1997.
11. Christensen TG, Draeby C. Models of the blood transport system. In: *Applied Mathematical Models in Human Physiology*. Philadelphia: Society for Industrial and Applied Mathematics, 2004, p. 168–180.
12. Coleman TG, Randall JE. HUMAN. A comprehensive physiological model. *Physiologist* 26: 15–21, 1983.
13. Comroe JH. Alveolar ventilation. In: *Physiology of Respiration*. Chicago: Year Book Medical Publishers, 1977, chapt. 2, p. 8–21.
14. Comroe JH. Mechanical factors in breathing. In: *Physiology of Respiration*. Chicago: Year Book Medical Publishers, 1977, chapt. 10, p. 91–141.
15. D'Angelo E, Agostoni E. Continuous recording of pleural surface pressure at various sites. *Respir Physiol* 19: 356–368, 1973.
16. Danielson M, Ottesen JT. Cardiovascular model. In: *Applied Mathematical Models in Human Physiology*, edited by Ottesen JT, Olufsen MS, Larsen JK. Philadelphia: Society for Industrial and Applied Mathematics, 2004, p. 115–118.
17. Drzewiecki G, Field S, Moubarak I, Li JK. Vessel growth and collapsible pressure-area relationship. *J Appl Physiol* 273: 2030–2043, 1997.
18. Duffin J. Model validation and control issues in the respiratory system. In: *Mathematical Modeling and Validation in Physiology: Applications to the*

- Cardiovascular and Respiratory Systems*, edited by Batzel JJ, Bachar M, Kappel F. New York: Springer Verlag, 2013, p. 133–162.
20. Duffin J, Mohan RM, Vasilou P, Stephenson R, Mahamed S. A model of the chemoreflex control of breathing in humans: model parameters measurement. *Respir Physiol* 120: 13–26, 2000.
 21. Eckberg DL. Point:counterpoint: respiratory sinus arrhythmia is due to a central mechanism vs. respiratory sinus arrhythmia is due to the baroreflex mechanism. *J Appl Physiol* (1985) 106: 1740–1742, 2009.
 - 21a. Edwards Lifesciences. *Normal Hemodynamic Parameters and Laboratory Values* (Online). <http://ht.edwards.com/scin/edwards/eu/sitecollectionimages/edwards/products/presep/ar04313hemodynpoCKETcard.pdf> [4 April 2014].
 22. Ellwein LM, Tran HT, Zapata C, Novak V, Olfesen MS. Sensitivity analysis and model assessment: mathematical models for arterial blood flow and blood pressure. *Cardiovasc Eng* 8: 94–108, 2008.
 23. Ferris BG, Mead J, Opie LH. Partitioning of respiratory flow resistance in man. *J Appl Physiol* 19: 653–658, 1979.
 24. Flumerfelt RW, Crandall ED. An analysis of external respiration in man. *Math Biosci* 3: 205–230, 1968.
 25. Fuhrman BP. Cardiopulmonary interactions. In: *Pediatric Critical Care*. Maryland Heights, MO: Mosby, 2011, p. 306–318.
 26. Fukui Y. *A Study of the Human Cardiovascular-Respiratory System Using Hybrid Computer Modeling* (PhD thesis). Madison, WI: University of Wisconsin, 1972.
 27. Giannessi M, Chbat NW, Den Buijs JH, Albanese A, Ursino M. Cardiovascular changes in cardiogenic and obstructive shocks: analysis using a cardiopulmonary simulation model. *Comput Cardiol* 35: 457–460, 2008.
 28. Goda K, Sasaki E, Nagata K, Fukai M, Ohsawa N, Hahafusa T. Pancreatic volume in type 1 and type 2 diabetes mellitus. *Acta Diabetol* 38: 145–149, 2001.
 29. Grimby G, Takishima T, Graham W, Macklem P, Mead J. Frequency dependence of flow resistance in patients with obstructive lung disease. *J Clin Invest* 47: 1455–1465, 1968.
 30. Grodins FS. Integrative cardiovascular physiology: a mathematical synthesis of cardiac and blood vessel hemodynamics. *Q Rev Biol* 34: 93–116, 1959.
 31. Grodins FS, Gray JS, Schroeder KR, Norins AL, Jones RW. Respiratory responses to CO₂ inhalation: a theoretical study of nonlinear biological regulator. *J Appl Physiol* 7: 283–308, 1954.
 32. Guyton AC, Coleman TG, Granger HJ. Circulation: overall regulation. *Annu Rev Physiol* 34: 13–46, 1972.
 33. Guyton AC, Hall JE. *Textbook of Medical Physiology*. Philadelphia: Elsevier Saunders, 2006.
 34. Heldt T, Shim EB, Kamm RD, Mark RG. Computational modeling of cardiovascular response to orthostatic stress. *J Appl Physiol* 92: 1239–1254, 2002.
 35. Hemalatha K, Manivannan M. Cardiopulmonary model to study interaction hemodynamics in mueller maneuver. *Int J Numer Meth Biomed Engng* 27: 1524–1544, 2011.
 36. Hester RL, Brown AJ, Husband L, Iliescu R, Pruett D, Summers RL, Coleman TG. Hummod: a modeling environment for the simulation of integrative human physiology. *Front Physiol* 2: 12, 2011.
 37. Ikeda N, Marumo F, Shirataki M, Sato T. A model of overall regulation of body fluids. *Ann Biomed Eng* 7: 135–166, 1979.
 38. Kiely KG, Cargill RI, Lipworth BJ. Effect of hypercapnia on hemodynamic, inotropic, lusitropic, and electrophysiologic indices in human. *Chest* 109: 1215–1221, 1996.
 39. Lin KH, Cumming G. A model of time-varying gas exchange in the human lung during a respiratory cycle at rest. *Respir Physiol* 17: 93–112, 1973.
 40. Liu YH, Bahn RC, Ritman EL. Myocardial volume perfused by coronary artery branches—a three-dimensional X-ray CT evaluation in human cadaver hearts. *Int J Card Imaging* 8: 95–101, 1992.
 41. Lu K, Clark JW, Ghorbel FH, Robertson CS, Ware DL, Zwischenberger JB, Bidani A. Cerebral autoregulation and gas exchange studied using a human cardiopulmonary model. *Am J Physiol Heart Circ Physiol* 286: H584–H601, 2004.
 42. Lu K, Clark JW, Ghorbel FH, Ware DL, Bidani A. A human cardiopulmonary system model applied to the analysis of the valsalva maneuver. *Am J Physiol Heart Circ Physiol* 281: H2661–H2679, 2001.
 43. Lu K, Clark JW, Ghorbel FH, Ware DL, Zwischenberger JB, Bidani A. Whole-body gas exchange in human predicted by a cardiopulmonary model. *Cardiovasc Eng* 3: 1–19, 2003.
 44. Magosso E, Ursino M. A mathematical model of CO₂ effect on cardiovascular regulation. *Am J Physiol Heart Circ Physiol* 281: H2036–H2052, 2001.
 45. Magosso E, Ursino M. Cardiovascular response to dynamic aerobic exercise: a mathematical model. *Med Biol Eng Comput* 40: 660–674, 2002.
 46. Mecklenburgh JS, Mapleson WW. Ventilatory assistance and respiratory muscle activity. 2: simulation with an adaptive active (“aa” or “a-squared”) model lung. *Br J Anaesth* 80: 434–439, 1998.
 47. Mengesha YA. Variability of cardiovascular responses to hypercapnia in man. *Ethiop J Health Dev* 14: 135–141, 2000.
 48. Michard F. Changes in arterial pressure during mechanical ventilation. *Anesthesiology* 103: 419–428, 2005.
 49. Neal ML, Bassingthwaite JB. Subject-specific model estimation of cardiac output and blood volume during hemorrhage. *Cardiovasc Eng* 7: 97–120, 2007.
 50. Nucci G, Cobelli C. Mathematical models of respiratory mechanics. In: *Modelling Methodology for Physiology and Medicine*, edited by Carson E. and Cobelli C. San Diego, CA: Academic, 2001.
 51. Proctor DF. Physiology of the upper airway. In: *Handbook of Physiology. Respiration*, edited by Fenn WO and Rahn H. Washington, DC: American Physiological Society, 1964, sect. 3, vol. 1, chapt. 8, p. 309–345.
 52. Putensen C. Inverse ratio ventilation. In: *Mechanical Ventilation: Clinical Applications and Pathophysiology*, edited by Papadakos P. and Lachmann B. Philadelphia: Saunders, 2008.
 53. Reynolds WJ, Milhorn HT Jr. Transient ventilatory response to hypoxia with and without controlled alveolar PCO₂. *J Appl Physiol* 35: 187–196, 1973.
 54. Reynolds WJ, Milhorn HT Jr, Holloman GH. Transient ventilatory response to graded hypercapnia in man. *J Appl Physiol* 33: 47–54, 1972.
 55. Rideout VC. *Mathematical and Computer Modeling of Physiological Systems*. Upper Saddle River, NJ: Prentice Hall, 1991.
 56. Rodrigues Júnior AJ, Rodrigues CJ, Germano MA, Rasera Júnior I, Cerri GG. Reproducibility of human kidney perfusion and volume determinations with electron beam computed tomography. *Invest Radiol* 31: 204–210, 1996.
 57. Rodrigues Júnior AJ, Rodrigues CJ, Germano MA, Rasera Júnior I, Cerri GG. Sonographic assessment of normal spleen volume. *Clin Anat* 8: 252–255, 1995.
 58. Ruskin J, Bache RJ, Rembert JC, Greenfield JC Jr. Pressure-flow studies in man: effect of respiration on the left ventricular stroke volume. *Circulation* 48: 79–85, 1973.
 59. Shen W, Punyanitya M, Wang Z, Gallagher D, St Omge MP, Albu J, Heymsfield SB, Heshka S. Total body skeletal muscle and adipose tissue volumes: estimation from a single abdominal cross-sectional image. *J Appl Physiol* 97: 2333–2338, 2004.
 60. Spencer JN, Firouzdale E, Mellins RB. Computational expressions for blood oxygen and carbon dioxide concentration. *Ann Biomed Eng* 7: 59–66, 1979.
 61. St Croix CM, Cunningham DA, Paterson DH. Nature of the interaction between central and peripheral chemoreceptor drives in human subjects. *Can J Physiol Pharmacol* 74: 640–646, 1996.
 62. Steinback CD, Salzer D, Medeiros PJ, Kowalchuk J, Shoemaker K. Hypercapnic vs. hypoxic control of cardiovascular, cardiovagal, and sympathetic function. *Am J Physiol Regul Integr Comp Physiol* 296: R402–R410, 2009.
 63. Thompson JE, Jaffe MB. Capnographic waveforms in the mechanically ventilated patient. *Respir Care* 50: 100–108, 2005.
 64. Timischl S. *A Global Model of the Cardiovascular and Respiratory System* (PhD thesis). Graz, Austria: Karl-Franzens Universitat, 1998.
 65. Timmons W. Cardiovascular models and control. In: *The Biomedical Engineering Handbook*, edited by Bronzino JD. Boca Raton, FL: CRC, 2000.
 66. Topor ZL, Vasilakos K, Younes M, Remmers JE. Model based analysis of sleep disordered breathing in congestive heart failure. *Respir Physiol Neurobiol* 155: 82–92, 2007.
 67. Ursino M. Interaction between carotid baroregulation and the pulsating heart: a mathematical model. *Am J Physiol Heart Circ Physiol* 275: H1733–H1747, 1998.
 68. Ursino M, Magosso E. A theoretical analysis of the carotid body chemoreceptor response to O₂ and CO₂ pressure changes. *Respir Physiol Neurobiol* 130: 99–110, 2002.
 69. Ursino M, Magosso E. Acute cardiovascular response to isocapnic hypoxia. I. A mathematical model. *Am J Physiol Heart Circ Physiol* 279: H149–H165, 2000.
 70. Ursino M, Magosso E, Avanzolini G. An integrated model of the human ventilatory control system: the response to hypercapnia. *Clin Physiol* 21: 447–464, 2001.
 71. van Meurs W. *Modeling and Simulation in Biomedical Engineering: Applications in Cardiorespiratory Physiology* (1st ed.). New York: McGraw-Hill Education, 2011.
 72. West JB. *Respiratory Physiology: The Essentials*. Philadelphia: Lippincott Williams & Wilkins, 2008.
 73. Westerhof N, Lankhaar JW, Westerhof BE. The arterial Windkessel. *Med Biol Eng Comput* 47: 131–141, 2009.